Yokohama National University

Enhanced Performance of Organic Solar Cells with Anode and Cathode Surfaces Treated by Molecular Self-Assembly and Ultrathin Layer

Byambasuren Delgertsetseg

2015

Contents

Chapter 1

General Introduction

A solar cell, or photovoltaic (PV) cell, is an electrical device, which converts the energy of light directly into electricity by PV effect. The "*photo"* means that light, and "*voltaic"* means that electricity, so the PV cell creates electricity from light. The PV effect is a basic physical process through which the PV cell converts the sunlight into electricity. Physicist A. E. Becquerel [1] first described the PV effect in 1839, but it remained a curiosity of science for the next three quarters of a century. In 1883, the first construction of solar cell with 1 % of power conversion efficiency (η_P) was reported by Charles Fritts, using selenium semiconductor coated in a thin layer of gold. In 1954, researchers from Bell laboratories depended on the Czochralski process to develop the first crystalline silicon PV cell, which had η_P of 4 %.

In recent years, PV cells based on organic semiconductors have attracted much attention. Organic PV cells are divided into three main categories depending on their technology. The first one is based on conjugated polymers is the so-called bulk-hetero-junction (BHJ) organic PV cells [2,3], the second one is based on small-molecular weight (thin-film) organic PV cells [4], and the last one the dye-sensitized solar cell (DSSC) [5]. The main differences between these three technologies are the fabrication methods employed and the types of materials.

Polymer based BHJ organic PV cells are typically made by solution processing of two conjugated polymers or one conjugated polymer and a C_{60} derivative, [6,6]-phenyl-C_{61}-butyric acid methyl ester (PCBM).

Small-molecular weight organic PV cells are typically fabricated by sublimating successive layers of hole and electron transporting materials under vacuum. DSSC cells are based on a semiconductor formed between a photo-sensitized electrode and an electrolyte, a photo electrochemical system. In 1991, DSSCs, introduced by Michael Grätzel [5] and coworkers, create a new paradigm for photon capture and charge transport in solar conversion.

In polymer based BHJ PV cells, the most common donor polymers that have been used in the past are poly[2-methoxy-5-(3,7-dimethyloctyloxy)-1,4-phenylene vinylene] (MDMO-PPV) [23-25], regioregular poly(3-hexylthiophene) (RR-P3HT) [26-33], and poly[2-methoxy-5-(2′-ethylhexyoxy)-1,4-phenylene vinylene] (MEH-PPV) [2, 17,18]. The most common candidate for the acceptor material is [6,6]-phenyl C_{61}-butyric acid methyl ester (PCBM) [19]. On the other hand, several small molecules such as copper phthalocyanine (CuPc) [20-22], zinc phthalocyanine (ZnPc) [23,24], tetracene [25], and pentacene [26] have been used as donors combined with Buckminsterfullerene (C_{60}) molecules in a bilayer HJ. The η_p reported so far for polymer based BHJ organic PV cells is close to 5 %, for devices based P3HT [14-16]. For small-molecule-based solar cells, η_p up to 6.0% have been reported for devices based on CuPc [21]. As a result of continuing research efforts, the efficiencies of organic PVs are now fast approaching the levels where they could be put into commercial applications.

Since C. W. Tang reported the first efficient donor-acceptor (D-A) hetero-junction (HJ) (also this structure is named as a two-layer) thin-film organic PV cell in 1986 [27], the organic semiconductor thin-film materials have been attracted much attention, due to their ease of fabrication, potential for low-cost productions, and compatibility with flexible substrates [28-32].

In typically, active layers of organic PV cells contribute to light absorption and current generation, generally consist of two types of organic semiconductor molecules, as named as a donor and an acceptor [33]. Therefore, many research groups have synthesized new materials for use as the donor and acceptor and utilized them for organic PV cells [33]. These attempts have produced promising materials that have shown a relatively high η_P of 7–10 % in organic PV cells [33-43].

In order to maximize the device performance of organic PV cells, the optical and electrical properties of the materials in bulk, and the interfaces of materials are key role to fully bring out

the abilities of the materials [43-45]. The contact properties at the interfaces between organic materials and electrodes (either ohmic or non-ohmic contact) should determine charge extraction efficiency under current flow conditions. Therefore, contact properties at the interface between organic material and electrode could be one cause of the major loss in photocurrent [33, 46,47].

In addition, the organic material/electrode interface is also related to charge recombination under an open-circuit condition, which could affect the potential difference in the photo-irradiated steady state. To understand full advantage of the superior properties of organic materials for organic PV cells, the charge extraction efficiency and recombination rate at the electrode interface should be optimized to achieve a high short-circuit current density (J_{sc}) and a higher open-circuit voltage (V_{oc}) [33].

This thesis describes improvements of the device performance of organic PV cells by controlling the work function (WF) of anode electrode to enhance charge collection and ohmic contact at the interface between anode and photo-active organic or polymer layer. This thesis also describes the further improvement of V_{oc} and built-in potential (V_{bi}) which is

defined by energy difference between WFs of anode and cathode electrodes to enhance the device performance. In order to improve to the V_{oc} and V_{bi}, we examined to increase the WF of anode and also reduce the WF of cathode electrode by chemical modification and introducing an ultra-thin buffer layer [48, 49].

In Chapter 1, General background of the study of organic photovoltaic (PV) cells has been described with in connection with the contents of the thesis.

In chapter 2, ITO anode is used for anode electrode in organic PV cells. The ITOs were chemically modified by *p*-substituted benzenesulfonyl chlorides with different terminal groups of H- and Cl- with different WFs. The energy offset at the ITO/zinc phthalocyanine (ZnPc) as a donor interface is fine-tuned widely depending upon the interface dipoles and thus correlation between the change in the WF of ITO and the device performance by chemical modification is discussed.

In chapter 3, The effect of the chemical modification of ITOs with CH_3O-, H-, Cl-, CF_3-, and NO_2-terminated *p*-benzenesulfonyl chlorides on the performance of bulk HJ PV cells based on poly(3-hexylthiophene) and [6,6]-phenyl-C_{61}-butyric acid methyl ester (P3HT:PC_{61}BM) composite structure is examined. Moreover, the contact properties at the interface between chemically modified ITO anode/ P3HT on the PV characteristics (J_{sc}, V_{oc}, fill factor (*FF*), and η_P) of bulk HJ PV cells based on poly(3-hexylthiophene) and [6,6]-phenyl-C_{61}-butyric acid methyl ester (P3HT:PC_{61}BM) is discussed in detail.

In chapter 4, Detailed investigation of increase in V_{oc} by controlling the WFs of anode and cathode electrodes is examined. The use of chemically modified ITO with different terminal groups (H- and Cl-) of *p*-benzensulfonyl chlorides forming effective monolayer and 4-chlorophenyldichorophospate (-P) is examined. The correlation between the change in the WFs of electrodes and the performance of the organic PV cells is discussed. In this study, we

demonstrate that the large increase in V_{oc} with increase in V_{bi}. The tris(8-hydroxyquinoline)aluminum (Alq_3) as an electron transport layer (ETL) to substitute for bathocuproine (BCP) is selected in organic PV cells based on rubrene(Rub)/buckminsterfullerene (C_{60}) HJ. In order to achieve the further improvement of V_{oc}, a lithium carboxylate (C_6H_5COOLi) [50] ultra-thin buffer layer (as a cathode interface) with low WF is inserted between ETL and Al is studied.

In chapter 5, BCP has been known as one of the most effective electron-transport layer material. However, the mechanism of the electron transport is not clear yet. In order to clarify this, organic PV cells of ITO/ZnPc/C_{60}/BCP/Au is formed with a laminated top electrode to suppress cathode-induced defect states in the BCP layer. The formation of the cathode-induced defect states below the LUMO of BCP is discussed. The efficient electron transport should be discussed *via* the lowest unoccupied molecular orbital (LUMO) energy level of BCP. The vacuum level shifts at the Au/BCP and BCP/C_{60} interfaces will be considered to be important factors to understand the effective electron transport via the LUMO of BCP layer.

In chapter 6, All the results of the research work was summarized in this chapter.

1.1. Basic operating principles in solar cell

Various architectures for organic PV cells have been investigated in recent years. **Fig. 1.1** shows the Metal/Insulator/Metal (MIM) type of widely used organic PV cells. One metal is optically transparent electrode like indium-tin-oxide (ITO) and the other metal is mostly made of Al or Ag deposited by vacuum evaporation. An insulator layer consists of organic semiconductor materials. The basic mechanism of photocurrent generation in organic PV cells can be illustrated with two organic materials; one is a donor and the other an acceptor. The conversion of solar light into electric power requires the generation of both negative and

positive charges as well as driving force that can push these charges through an external electric circuit.

There are four main steps involved in the photon to conversion mechanism for the PV cells. **Fig.1.1** also shows the steps in the photocurrent generation process of PV cell. First step is absorption of light. When the light illuminate into the anode side, an electron in the donor undergoes photo-induced excitation from the highest occupied molecular orbital (HOMO) level to the lowest unoccupied molecular orbital (LUMO) level of the organic material, forming a Frenkel exciton (Coulombically bound electron (e-) and hole (h+)). The ratio of the generated Frenkel excitons to the total incident photons, in terms of energy, is defined as the absorption efficiency. Excitons in organic materials have a binding energy [51] of 0.5 – 1 eV, due to their low dielectric permittivity [51] ($\varepsilon = 3 - 4$). In comparison, thermal energy (kT) at a room temperature (298 K) is approximately 0.025 eV, substantially lower than the binding energy (0.5 – 1 eV) of an exciton in an organic material [52].

Thus, if the organic material is to serve as a donor in organic PV cells, a second material is required as an acceptor to ensure a built-in internal field at the interface to break up any excitons that diffuse there into free carriers. The most widely used acceptor materials are fullerenes, which have electron affinities greater than those of polymers or small molecules [52].

Second step is exciton diffusion. The excitons must diffuse to the donor-acceptor (D-A) interfaces within the diffusion length (L_D) to prevent recombining to the ground state. Because the value of L_D in organic materials [53] is typically 10 nm, the ideal donor or acceptor domain size is less than 20 nm. This D–A interface concept is analogous in terms of charge transport to a p-n junction in an inorganic semiconductor. The ratio of the number of

excitons that reach the D-A interface to the total number of excitons generated through photo-excitation is defined as the exciton diffusion efficiency [52].

Third step is charge separation or exciton dissociation. The exciton at a D–A interface undergoes charge transfer (CT) process at an ultrafast pace [54] (ca. 100 fs) to form a CT exciton, where the hole and electron remain in the donor and acceptor, respectively, held together through Coulombic attraction. The charge separation efficiency is defined as the ratio of the number of excitons that have undergone the CT process to the number of excitons that have reached the D–A interface.

Fourth step is charge transport, as a result of the built-in electric field, into free holes and electrons, which are then transported through the donor and acceptor, respectively, to their respective electrodes. The transport of free carriers to the respective electrodes occurs within a period of time ranging from nano- to microseconds. The charge collection efficiency is defined as the ratio of the number of carriers that have been collected at the electrodes to the number of excitons that have undergone the CT process.

Solar cells are further characterized by measuring the current density-voltage (*J*-*V*) curve under illumination of a light source that mimics the sun spectrum. In order to understand the rectifying behavior of an intrinsic carrier concentration organic semiconductor device, the MIM model [55] is useful. In **Fig. 1.2** semiconductor, sandwiched between two metal electrodes with different WFs is depicted for several situations.

In **Fig. 1.2 (a),** the current delivered by a solar cell under zero bias is J_{sc}. There is no voltage applied (i.e., short circuit conditions). Hence, there is no net current flowing in the dark, and the built-in electric field resulting from the difference in the electrode's WFs is evenly distributed throughout the device. Under illumination, separated charge carriers can

drift in this electric field to the respective contacts: the electrons move to the lower WF electrode and the holes to the opposite.

In **Fig. 1.2 (b),** the voltage where the current equals zero is called V_{oc}. In the MIM picture this situation is shown for open circuit conditions, also known as "flat band condition". The applied voltage, which corresponds in this case to the difference in the electrode work functions, balances the built-in field. As there is no net driving force for the charge carriers, the current is zero.

In **Fig. 1.2 (c),** when $V < 0$, the diode is driven under a reverse biased condition the solar cell works as a photo-detector and only a very small injected dark current can flow. Under illumination, the generated charge carriers drift under strong electric fields to the respective electrodes. The field, if higher than in **Fig. 1. 2 (a),** often leads to enhanced charge generation and /or collection efficiency.

In **Fig. 1.2 (d),** When $V > V_{oc}$ the diode is biased in the forward direction. If a forward bias larger than V_{oc} ($V > V_{oc}$), the contacts effectively inject charges into the semiconductor. If these can recombine, the device works as a light-emitting diode. Electrons are now injected from the low WF electrode into the lowest LUMO and holes from the high WF electrode into the HOMO of the organic layer, respectively.

1.2. The equivalent circuit analysis of photovoltaic cell

The equivalent circuit of PV cell [55] is shown in **Fig. 1.3**, and basis for its current density-voltage (*J-V)* characteristics. Generally, the *J-V* characteristics of a PV cell can be described by the following equation 1.1 [56].

$$J = J_S\left\{\exp\left(\frac{e}{nkT}(V - JR_S)\right) - 1\right\} + \frac{V - JR_S}{R_p} - J_{ph} \qquad (1.1)$$

where J is measured current, J_s is the reverse saturation currents density of the diode, n is the diode ideality factor, e is the electron charge, V the applied voltage, R_s and R_p are the series and parallel resistances, respectively, k is Boltzmann constant, T is absolute temperature in degrees Kelvin, and J_{ph} is the photocurrent density. In this way, two more characteristics could be extracted from the *J-V* curve. These are the cell's parallel (R_p) and series resistance (R_s). The parallel resistance is mainly the slope of the curve in the range around 0 V (3rd and 4th quadrant). At lower R_p the open circuit voltage drops, while J_{sc} stays the same (shown in **Fig. 1.3**). The serial resistance defines the slope of the *J-V* curve in 1st quadrant, i.e in the range above the V_{oc} (transmitting direction of diode).

An ideal diode and solar cell, the R_s is very small and can ignore. Oppositely, the R_p is close to infinity and treats as open in the equivalent circuit. Therefore, the Eq.(1.2) is simplified as

$$J = J_S\left[\exp\left(\frac{eV}{nkT}\right) - 1\right] - J_{ph} \tag{1.2}$$

1.3. Electrical characterization of photovoltaic cell

The most widely used method for PV cell characterization is the *J-V* characteristic of the cells, or the so called *J-V* measurement. The *J-V* characteristics of PV cell in the dark and under illumination are shown in **Fig. 1.4** and from such a curve, the basic performance parameters can be extracted as listed in **Table 1.1.** Under dark conditions the PV cell shows a diode behavior with a characteristic rectification ratio. When light is shined to the device the current raised at reverse bias, this called photocurrent.

The measurement of their *J-V* characteristics is done in the following way: during illumination, a voltage is applied on the electrodes of the cell and the flowing current is measured. In the dark, the *J-V* curve passes through the origin-with no potential, no current flows. The most important parameters on this cell are the V_{oc}, J_{sc}, *FF*, and η_p. One of these parameters is the J_{sc}, which is determined on that *V* is equal to zero by Eq.(1.2) and the point where the curve cuts the Y axis (shown in **Fig. 1.4**). This equals to the photo current J_{ph} ideally. This is the current that flows through an illuminated PV cell when there is no external resistance (i.e., when the electrodes are simply connected or short-circuited). The short-circuit current is the maximum current that a device is able to produce. Under an external load, the current density will always be less than J_{sc}.

The second parameter is the V_{oc}, which is the intersection of the *J-V* curve (see **Fig. 1.4**) with the X axis, and the maximum possible voltage across a PV cell; the voltage across the cell in sunlight when no current is flowing. Setting *J* to zero in Eq. (1.2) gives the ideal value. The relation between V_{oc} and J_{sc} can be determined when it is assumed those $R_s = 0$ and $R_p = \propto$, with $J = 0$ and $J_{ph} = J_{sc}$:

$$V_{oc} = \frac{kT}{e} \ln\left(\frac{J_{ph}}{J_s} + 1\right) \tag{1.3}$$

V_{oc} is determined by the properties of the semiconductor by virtue of its dependence on J_s.

The third parameter is the *FF*, which is defined as the ratio of the maximum power ($J_{mpp} \times V_{mpp}$) divided by the J_{sc} and V_{oc} in light *J-V* characteristics of solar cells. This is a key quantity used to measure cell performance. The formula for *FF* in terms of the above quantities is:

$$FF = \frac{J_{mpp} V_{mpp}}{J_{sc} V_{oc}} = \frac{P_{max}}{J_{sc} V_{oc}} \tag{1.4}$$

where V_{mpp} and J_{mpp} are the voltage (V) and current density (mA cm^{-2}), respectively, at the cell maximum power point (P_{max}). The maximum power point is the point on the J–V curve where the area of the resulting rectangle is largest.

$$P_{max} = J_{mpp} V_{mpp} \tag{1.5}$$

Next important parameter is η_P. The ratio of power output to power input. In other words, η_P measures the amount of power produced by a solar cell relative to the power available in the incident solar radiation (P_{in}). The power conversion efficiencies of the cell under simulated AM1.5 G conditions were calculated according to the relation:

$$\eta_p = \frac{J_{mpp} V_{mpp}}{P_{in}} = \frac{FF\, J_{sc} V_{oc}}{P_{in}}; \tag{1.6}$$

P_{in} –incident light intensity on the solar cell and is generally fixed at 100 Wcm^{-2} when a solar simulator is used.

1.4. Device structure of organic photovoltaic cell

Organic PV cells comprising two components, a donor and an acceptor material. Charge separation occurs at the interface between those two. For example, in the case of D-A devices, an acceptor material with good electron conductivity and a donor material with good hole conductivity are ideal.

Transparent ITO is usually used as an anode electrode (hole collecting electrode). The top electrode (electron collecting electrode) is usually made of Au, Ag or Al thin-film layers deposited *via* physical vapor deposition. Ideally, the donor material should only be in contact with the electrode material with the higher WF (typically ITO) and the acceptor material with the lower WF electrode (typically Al). **Fig.1.5** shows two different types of donor and acceptor architecture for organic PV cells.

Two-layer (bilayer) cells. This structure benefits from the separated charge transport layers that ensure connectivity with the correct electrode and give the separated charge carriers only little chance to recombine with its counterpart. The drawback is the small interface that allows only excitons of a thin layer to reach it and get dissociated.

Blend cell. The strong point of this type is the large interface area if the molecular mixing occurs on a scale that allows good contact between alike molecules (charge percolation) and most excitons to reach the D-A interface. This can usually only be partly achieved so the defects of the network structure-particularly the connectivity with the correct electrode-represents a technological challenge.

1.5. Purpose of study

2. Energy level tuning at the WF of ITO anode/HOMO of donor interface by using self-assembled monolayer (SAM) to enhance PV performance of small-molecule organic PV cell;
3. To investigate the dependencies of the PV performance of poly(3-hexylthiophene) (P3HT)/[6,6]-phenyl-C61-butyric acid methyl ester (PC61BM) based BHJ organic PV cells with ITO anode WF modified with SAM;
4. To study the effect of the WF change of ITO anode and Al cathode electrodes on the Voc to enhance PV performance of small-molecule organic PV cell;

5. To study the effect of bathocuproine (BCP) electron-transport layer in small-molecule organic PV cells with laminated top electrode to improve PV performance.

References

[1]. A. E. Becquerel, Comt. Rend. Acad. Sci. **9**, 561 (1839).

[2]. G. Yu, J. Gao, J. C. Hummelen, F. Wudl, and A. J. Heeger, Science. **270**, 1789 (1995).

[3]. N. S. Saraciftci, L. Smilowitz, A. J. Heeger, and F. Wudl, Science. **258**, 1474 (1992)

[4]. B. P. Rand, J. Genoe, P. Heremans, J. Poortmans, Prog. Photovolt: Res. Appl. **15**, 659 (2007).

[5]. B. O'Regan and M. Grätzel, Nature (London). **353**, 737 (1991).

[6]. L. J. Lutsen, P. Adriaensens, H. Becker, A. J. Van Breemen, D. Vanderzande, and J. Gelan, Macromolecules. **32**, 6517 (1999).

[7]. S. E. Shaheen, C. J. Brabec, F. Padinger, T. Fromherz, J. C. Hummelen, and N. S. Sariciftci, Appl. Phys. Lett. **78**, 841 (2001).

[8]. M. M. Wienk, J. M. Kroon, W. J. H. Verhees, J. Knol, J. C. Hummelen, P. A. van Hal, R. A. J. Janssen, Angew. Chem. Int. Ed. **42**, 3371 (2003).

[9]. T. Chen, and R. D. Rieke, J. Am. Chem. Soc. **114**, 10 087 (1992).

[10]. R. D. McCullough, R. D. Lowe, M. Jayaraman, and D. L. Anderson, J. Org. Chem. **58**, 904 (1993).

[11]. F. Padinger, R. S. Rittberger, and N. S. Sariciftci, Adv. Funct. Mater. **13**, 85 (2003).

[12]. D. Chirvase, J. Parisi, J. C. Hummelen, and V. Dyakonov, Nanotechnology. **15**, 1317 (2004).

[13]. G. Li, V. Shrotriya, Y. Yao, and Y. Yang, J. Appl. Phys. **98**, 043704 (2005).

[14]. G. Li, V. Shrotriya, J. Huang, Y. Yao, T. Moriarty, K. Emery, and Y. Yang, Nat. Mater. **4**, 864 (2005).

[15]. M. Reyes-Reyes, K. Kim, and D. L. Carroll, Appl. Phys. Lett. **87**, 083506 (2005).

[16]. W. L. Ma, C. Y. Yang, X. Gong, K. Lee, and A. J. Heeger, Adv. Funct. Mater. **15**, 1617

(2005).

[17]. N. S. Sariciftci, D. Braun, C. Zhang, V. I. Srdanov, and A. J. Heeger, G. Stucky, F. Wudl, Appl. Phys. Lett. **62**, 585 (1993).

[18]. S. Alem, R. de Bettignies, J.-M. Nunzi, and M. Cariou, Appl. Phys. Lett. **84**, 2178 (2004).

[19]. J. C. Hummelen, B. W. Knight, F. LePeq, F. Wudl, J. Yao, and C. L. Wilkins, J. Org. Chem. **60**, 532 (1995).

[20]. P. Peumans, S. Uchida, and S. R. Forrest, Nature (London). **425**, 158 (2003).

[21]. J. Xue, S. Uchida, B. P. Rand, and S. R Forrest,. Appl. Phys. Lett. **85**, 5757 (2004).

[22]. F. Yang, M. Shtein, and S. R. Forrest, Nat. Mater. **4**, 37 (2005).

[23]. J. Drechsel, B. Männig, F. Kozlowski, D. Gebeyehu, A. Werner, M. Koch, K. Leo, and M. Pfeiffer, Thin Solid Films. **451**, 515 (2004).

[24]. J. Drechsel, B. Männig, D. Gebeyehu, M. Pfeiffer, K. Leo, and H. Hoppe, Org. Electron. **5**, 175 (2004).

[25]. C. W. Chu, Y. Shao, V. Shrotriya, and Y. Yang, Appl. Phys. Lett. **86**, 243 506 (2005).

[26]. S. Yoo, B. Domercq, and B. Kippelen, Appl. Phys. Lett. **85**, 5427 (2004).

[27]. C. W. Tang, Appl. Phys. Lett. **48**, 183 (1986).

[28]. B. P. Rand, J. Genoe, P. Heremans, J. Poortmans, Prog. Photovolt: Res. Appl. **15** 659-661. (2007).

[29]. T. Keitzke, Advances in OptoElectronics, 2007, 1 (Article ID 40285) (2007).

[30]. M. C. Scharber, D. Műhlbacher, M. Koppe, P. Denk, C. Waldauf, A. J. Heeger, and C. J. Brabec, Adv. Mater. **18**, 789 (2006).

[31]. S. E. Gledhill, B. Scott, and B. A. Gregg, J. Mater. Res. **20**, 3167 (2005).

[32]. S. Gűnes, H. Neugebauer, and N. Z. Sariciftci, Chem. Rev. **107**, 1324 (2007).

[33]. Phys. Chem. Chem. Phys., **14**, 3713 (2012).

[34]. H. Y. Chen, J. Hou, S. Zhang, Y. Liang, G. Yang, Y. Yang, L. Yu, Y. Wu and G. Li, Nat. Photonics, **3**, 649 (2009).

[35]. C. Piliego, T. W. Holcombe, J. D. Douglas, C. H. Woo, P. M. Beaujuge and J. M. J. Frechet, J. Am. Chem. Soc., **132**, 7595 (2010).

[36]. T. Y. Chu, J. Lu, S. Beaupre, Y. Zhang, J. R. Pouliot, S. Wakim, J. Zhou, M. Leclerc, Z. Li, J. Ding and Y. Tao, J. Am. Chem. Soc., **133**, 4250 (2011).

[37]. H. J. Son, W. Wang, T. Xu, Y. Liang, Y. Wu, G. Li and L. Yu, J. Am. Chem. Soc., **133**, 1885 (2011).

[38]. Z. He, C. Zhong, X. Huang, W. Y. Wong, H. Wu, L. Chen, S. Su and Y. Cao, Adv. Mater., **23**, 4636 (2011).

[39]. NREL, In http://www.nrel.gov/ncpv/

[40]. J Yang *et al.,* Adv Mater 23 (**30**), 3465 (2011).

[41]. V. S. Gevaerts *et al.,* Adv Mater 24 (16), 2130 (2013).

[42]. Kim, J. Y., et al. , Science 317 (**5835**), 222 (2007).

[43]. H. Ishii, K. Sugiyama, E. Ito and K. Seki, Adv. Mater., **11**, 605 (1999).

[44]. X. Y. Zhu and A. Kahn, MRS Bull., **35**, 443 (2010).

[45]. H. Ma, H. L. Yip, F. Huang and A. K. Y. Jen, Adv. Funct. Mater., **20**, 1371 (2010).

[46]. H. L. Yip, S. K. Hau, N. S. Baek, H. Ma and A. K. Y. Jen, Adv. Mater., **20**, 2376 (2008).

[47]. C. Ganzorig and M. Fujihira, Jpn. J. Appl. Phys., **38**,11B, pp. L1348 (1999).

[48]. K. Sarangerel, C. Ganzorig, M. Fujihira, M. Sakomura, K. Ueda, Chem. Lett. **37**, 778 (2008).

[49]. K. Sarangerel1, B. Delgertsetseg, N. Javkhlantugs, Masaru. Msakomura, C. Ganzorig, World Journal of Nano Scien. and Eng., **3**, 113 (2014).

[50]. S. R. Forrest, Nature **428** (6986), 911 (2004).

[51]. C. Deibel and V. Dyakonov, Rec Prog Phys **73** (9), 096401 (2010).

[52]. Y. W. Su, S. C. Lan, and K. Hwa, Materials Today, **15**, 554 (2012).

[53]. P. Peumans, *et al.* , J. Appl. Phys **93** (7), 3693 (2003).

[54]. C. J. Brabec *et al*., Chem. Phys. Lett **340** (3-4), 232 (2001).

[55]. S A. L. Fahrenbrach, and R. H. Bube, Fundamentals of solar cells, Academic, New York (1983).

[56]. H. C. Raus, Solar Cell Array Design Handbook, Van Nostrand Reinhold, New York 86, (1980).

[57]. M. Sze, Physics of Semiconductor Devices, John Wiley & Sons, New York (1981).

Figures and Tables

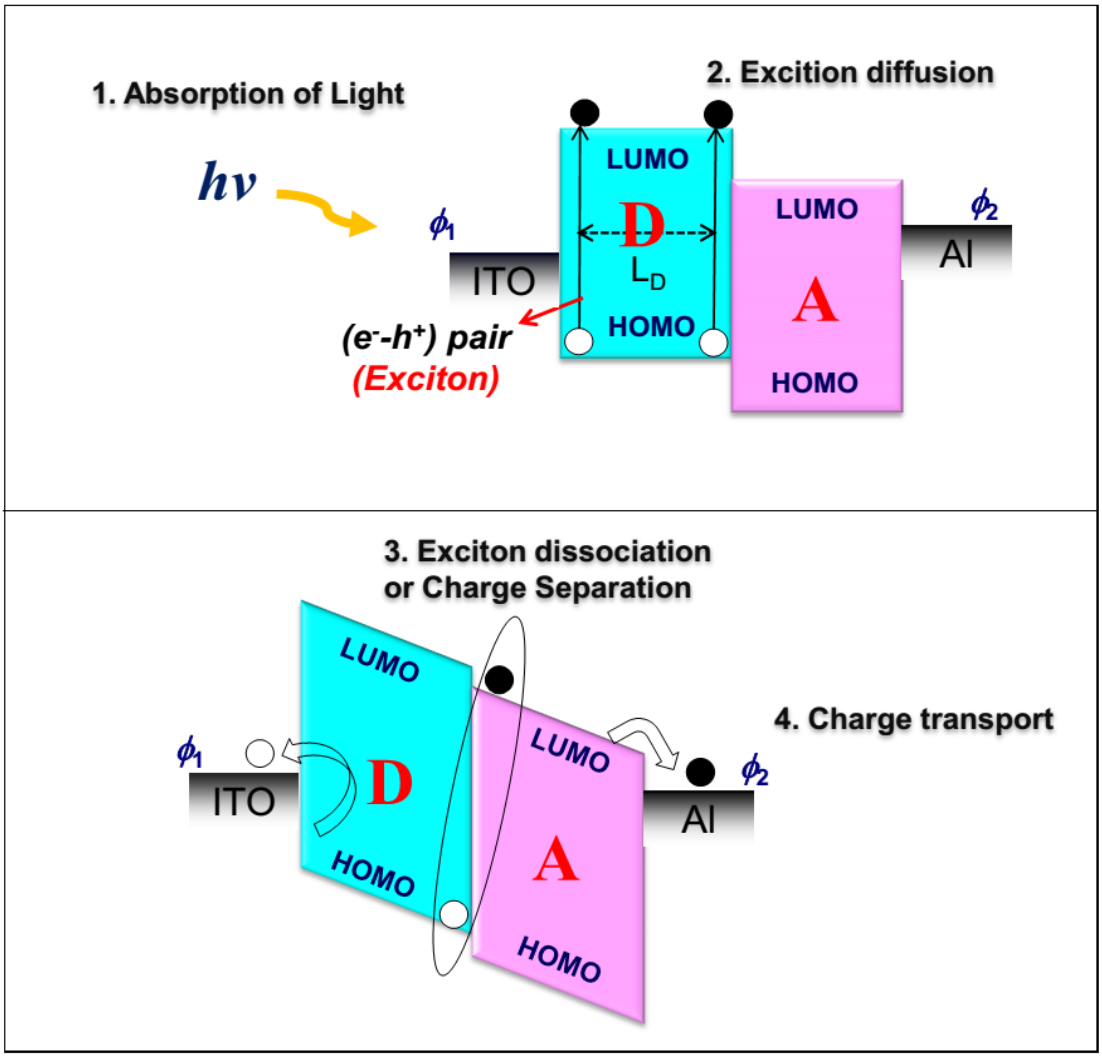

Fig. 1.1 Steps in the photocurrent generation process of Metal /Insulator/ Metal type organic PV cell. One metal is optically transparent electrode like ITO and the other metal is mostly made of Al deposited by vacuum evaporation. An insulator layer consists of organic semiconductor materials. One is a donor (D) and other is an acceptor (A). Here, LUMO is the lowest unoccupied molecular orbital, and HOMO is the highest occupied molecular orbital of the organic film.

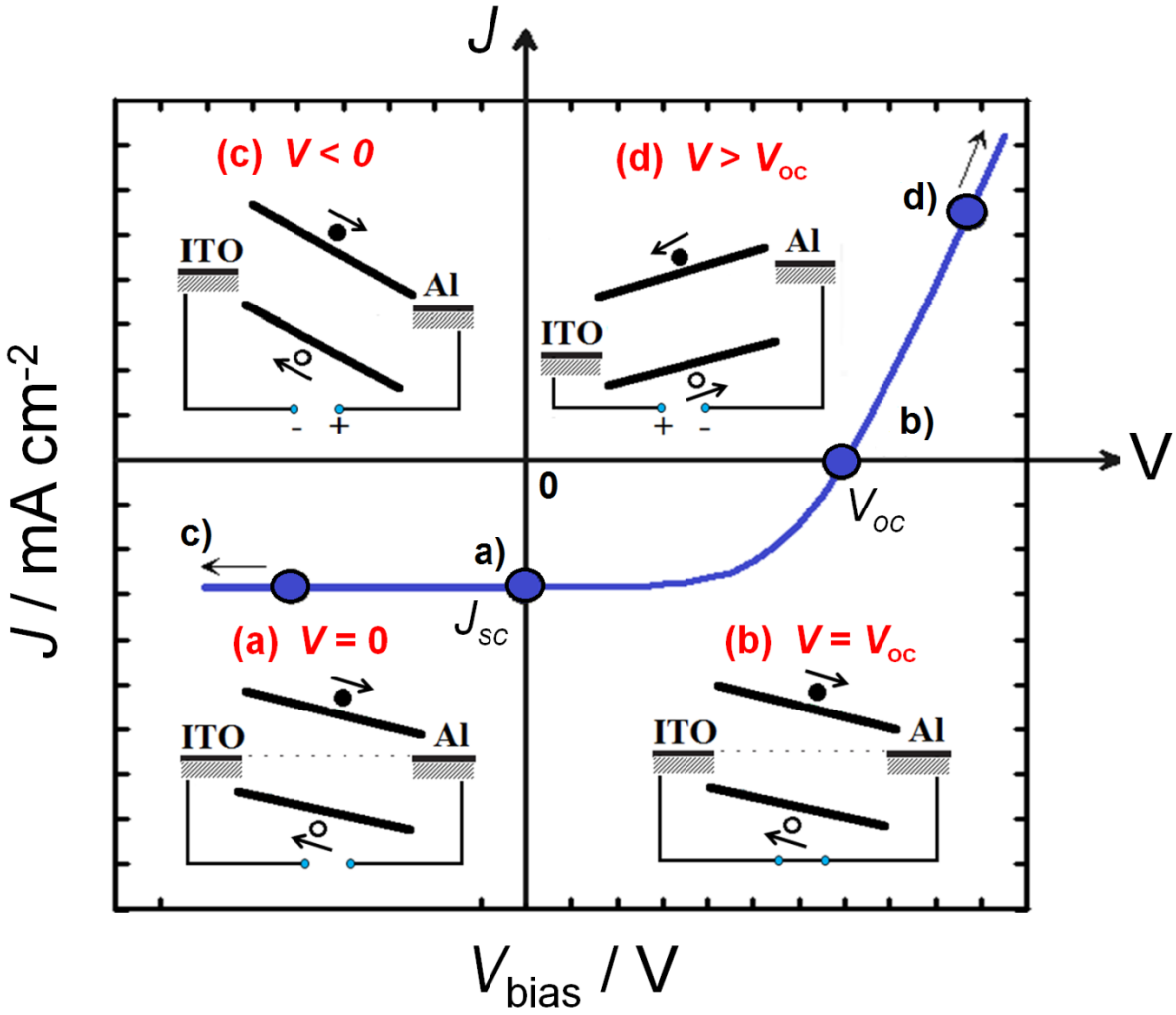

Fig. 1.2 Simple model that relates the *J-V* characteristics qualitatively to energy level diagrams. (a) Closed circuit condition (J_{sc}): under illumination photogenerated charges drift toward the contacts. (b) Open circuit condition (V_{oc}): the current becomes zero. (c) Reversed bias: photo generate charges drift in strong electric fields, the diode operates as a photodetector. (d) Forward bias larger than V_{oc}.

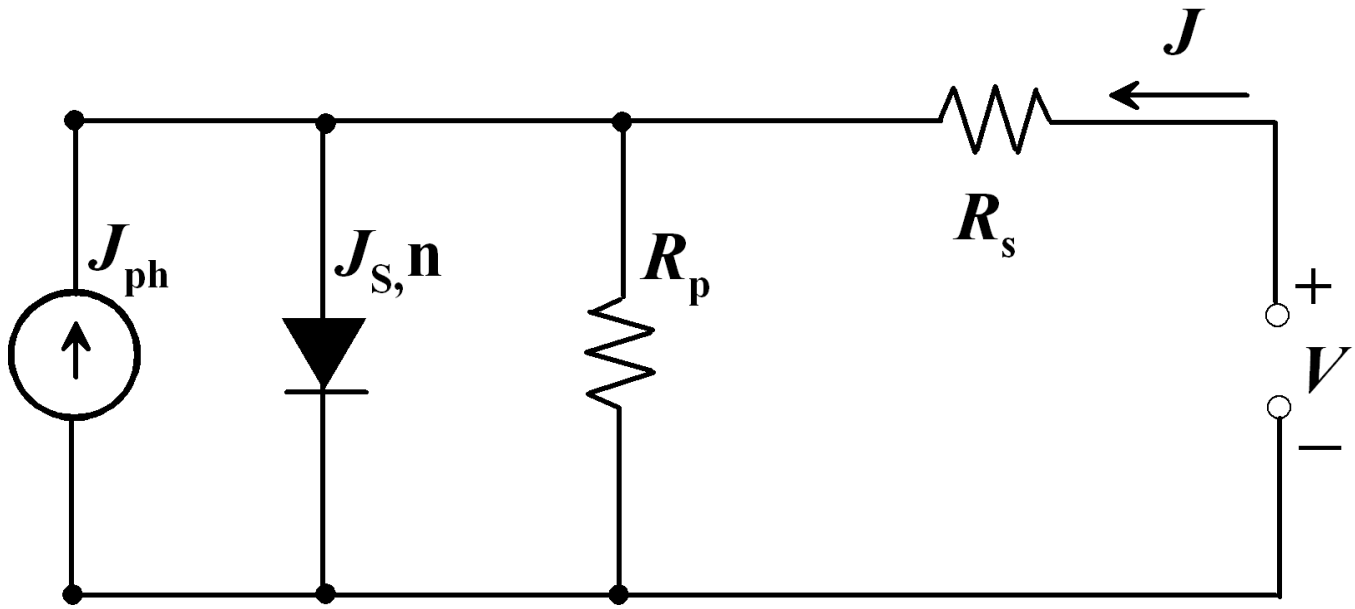

Fig. 1.3 Equivalent circuits for an organic PV cell. The series and parallel resistances are R_s and R_p, respectively, n is the diode ideality factor, and J_S and J_{ph} are the reverse saturation and photocurrent densities, respectively.

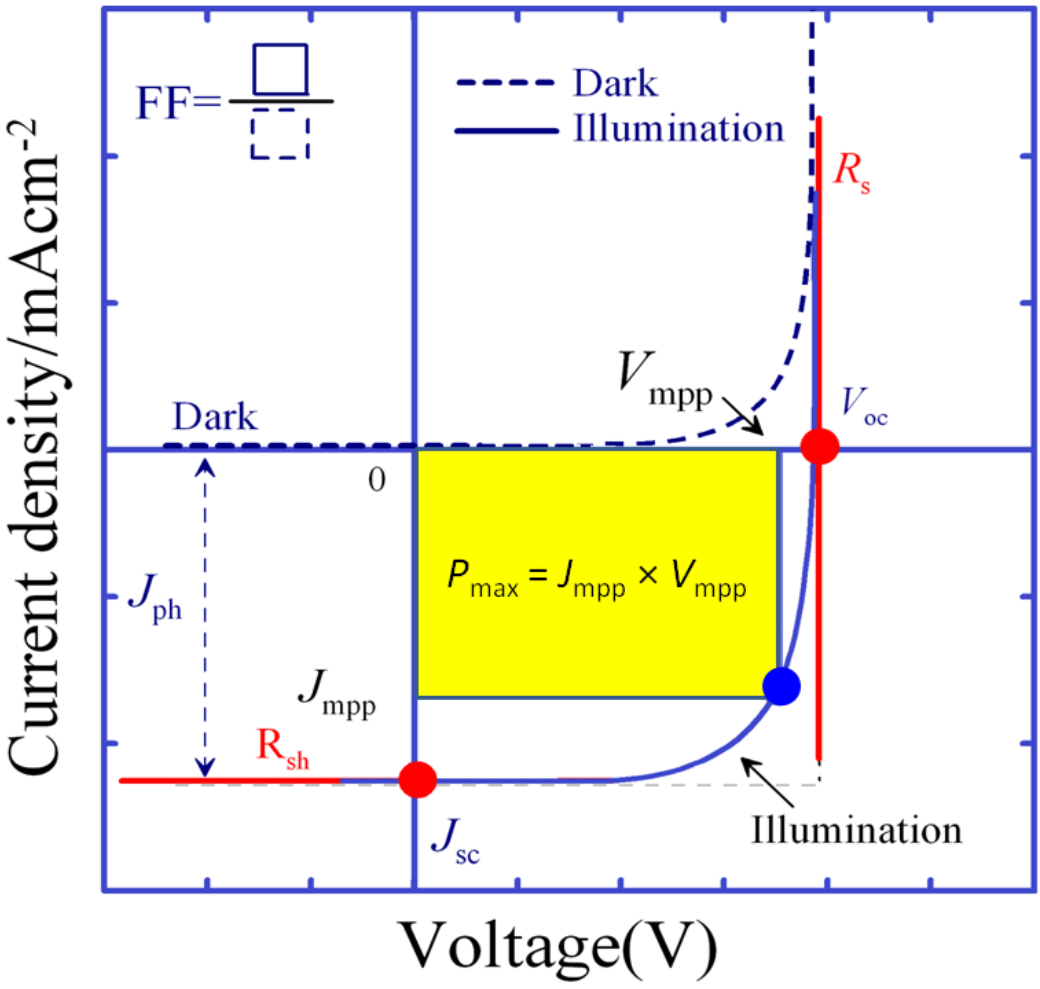

Figure 1.4 Typical **c**urrent density-voltage curves of organic solar cell (dark, dashed, illuminated, full line). The characteristic intersections with the abscissa and the ordinate are the open-circuit voltage (V_{oc}) and short circuit current (J_{sc}). The point of current and voltage (J_{mpp} and V_{mpp}, respectively.) corresponds to maximum power output. The rectangular region in the fourth quadrant indicates maximum power output.

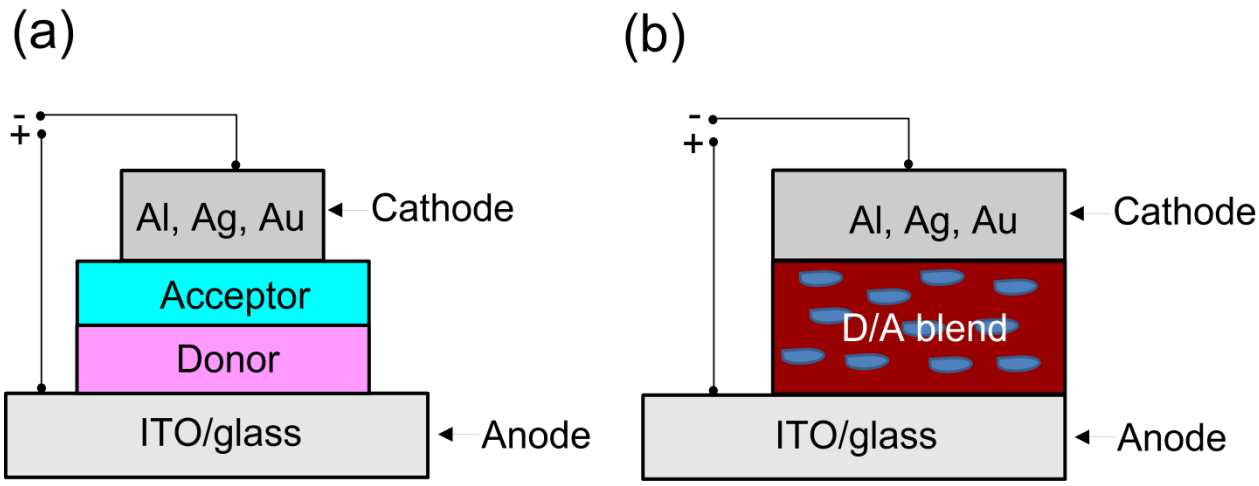

Fig.1.5. Two different types of donor and acceptor architecture for organic PV cells. (a). Two-layer structure consist of donor and acceptor which requires two separate deposition processes. (b). Blend structure can be obtained by spin coating using donor and acceptor mixture.

Chapter 2

Improved Performance of Organic Photovoltaic Cells with Indium-Tin-Oxide Electrode Treated by Self-Assembled Monolayer

2.1. Introduction

In recent years, a formation of molecular self-assembled monolayer (SAM) at electrode surfaces has been widely used for organic optoelectronic devices. How to bind molecules on electrode surfaces has been studied extensively among electrochemists since 1970s and as named as chemical modification of electrode surfaces [1-3]. Studies for formation of various organic monolayers with carboxylic and phosphonic acids as well as organosilanes on *n*-type transparent oxide electrode surfaces with wide band gap were reviewed and discussed comprehensively in Ref [4].

Indium-tin-oxide (ITO) has properties of high conductivity and transparency in the visible spectral region. The ITO is typically used for applications in organic photovoltaic (PV) cell [5] and organic light emitting diode (OLED) [6]. However, the work function (WF) of ITO is generally not sufficiently large for the contact to be ohmic and there is an energy barrier or step for hole injection from ITO to organic layer. Therefore, various surface treatments of ITO have been attempted to change the WF of ITO in order to control the energy step for hole injection reviewed in Ref. [7]. Fujihira and coworkers [8,9] carried out pioneering work on covalently attaching organic molecules with functional groups such as –COOH and –COCl binding groups onto SnO_2 surface. The latter was more reactive [9]. Wrighton and coworkers [10] took advantage of the selective surface attachment of carboxylic or phosphonic acid to ITO electrode and thiol to Au electrode. Zuppiroli and coworkers [11-15] observed improved

performance in the OLEDs using poly(para-phenylene)-functionalized carboxylic acid (PPP-func) [13], *p*-substituted benzoic acids [12-14], bicarbazyl-N,N'-dialkanoic acids [13], and 8-hydroxyquinoline-5-carboxylic acid [15] monolayers grafted to ITO electrode.

Using a similar approach Willis and coworkers demonstrated that the ITO electrode modification with 2-chloroethyl- [16] trichloromethyl-, aminomethyl-, and 4-nitrophenylphosphonic acids [17] greatly enhanced the device performance of OLED, most notably by reduction of turn-on voltages.

In our previous study, the acid chlorides [18-21] were used for chemical modification and the ITO surfaces were modified quickly and wide change in the WF of ITO was realized. The WF of ITO can be tuned by chemical modification of its surface with SO_2Cl–, COCl–, and –PO_2Cl_2 binding groups of *p*-substituted benzene derivatives [18]. n-Nonanoyl chloride and n-palmitoyl chloride were also used in Ref [19]. The chemical modification of ITO substrates for OLEDs [22-26] closely followed the procedure described in Ref. [18].

There are many other studies of ITO surface modification [4,7] for the purpose of enhanced charge injection and work function control in OLEDs. Although a number of groups have shown that chemical modification of ITO can be used to optimize the performance of OLEDs [11-26], there have been limited attempts to use chemical modification of ITO by SAM in organic PV cells.

Armstrong *et al.* used ferrocene dicarboxylic acid (Fc(COOH)2) and 3-thiophene acetic acid (3-TAA) to modify ITO films before they further modified these interfaces by electrochemically growing a thin layer of poly(3,4-ethylenedioxythiophene)/poly(styrene sulfonic acid) (PEDOT:PSS) [27,28]. The higher short-circuit currents observed in organic PV cells [28] using these chemically modified interfaces was attributed to better wettability of the organic layers compared to the polar ITO surface, and also enhanced transfer between the

ITO electrode and copper phthalocyanine layers by means of the charge intermediate PEDOT:PSS layer.

In this chapter, we studied the PV properties of organic PV cells deposited on ITO electrodes. For a typical device configuration of ITO/zinc phthalocyanine (ZnPc)/buckminsterfullerene (C_{60})/Al with and without bathocuproine (BCP) as an exciton blocking layer, the device performances, including short-circuit current density (J_{sc}), open-circuit voltage (V_{oc}), fill factor (FF), and power conversion efficiency (η_p) was examined. In addition, we compare the device characteristics before and after the surface modifications of ITO electrodes.

2.2. Experimental

2.2.1. Materials

In this work, we used zinc phthalocyanine ($C_{32}H_{16}N_8Zn$, "ZnPc") and buckminsterfullerene (C_{60}), respectively, as an electron and an electron acceptor of organic PV cell. Both ZnPc and C_{60} are commonly used materials for organic PV cell, and as such are relatively cheap and easy to obtain. The organic materials used in the device were ZnPc (purity ~97%, Aldrich), three times purified by thermal gradient sublimation prior to deposition and C_{60} (Tokyo Kasei Kogyo, purity >99%) and bathocuproine BCP (Kanto chemical, purity >99%) were used without further purification.

C_{60} is an *n*-type semiconductor material and one of the most profitable semiconductors used as an electron acceptor for the solar cells. Recently, bathocuproine ($C_{26}H_{20}N_2$, "BCP") has been extensively used as a buffer layer between an organic semiconductor and a metal electrode in organic PV cells. Metal electrode Al (Nilaco) was used as received.

2.2.2. Preparation of ITO

ITO coated glass substrates with a sheet resistance of ca. 15 Ω/square (Sanyo Vacuum Industries) were cut into 15 x 20 mm^2 sample slides. A 5 mm wide ITO strip line was formed by selective etching in vapor of solution made with hydrochloric acid (HCl) and nitric acid (HNO_3) with a volume ratio of 3:1 for 9 min at room temperature.

The patterned ITO substrates were cleaned by sonication successively in two kinds of detergents Extran MA (MERCK, 1 %) and Kontaminon O (WAKO Chemical Industries, Ltd, 5 %) in ultrasonic bath for 30 min for each detergent aqueous solution, respectively. After cleaning with the detergent, the ITO substrates were washed with a copious amount of line water cleaned and ultrasonicated successively in acetone and in isopropanol, each for 10 min and then were transferred to *i)* boiled isopropanol and *ii)* deionized water. Acetone and isopropanol were purchased from Kanto Chemical Co., Inc.

2.2.3. Chemical modification of ITO

After cleaning with isopropanol and deionized water the substrates (as-cleaned ITO) were for removing detergents. After words, the ITO substrate was stored under until being required. Prior to use, the substrates were further immersed for 30 min in dichloromethane (Kanto chemical Co., Inc) solutions containing 1mM of H- and Cl-terminated benzenesulfonyl chlorides. The modified ITOs were rinsed in pure dichloromethane and then vacuum dried for ~1 h [3].

2.2.4. Device fabrication procedure

The organic PV cells were fabricated using ZnPc and C_{60}. The BCP has a function of transporting electrons to the cathode from the adjoining acceptor layer of C_{60} while effectively

blocking excitons in the lower-energy-gap acceptor layer from recombining at the cathode [18]. For the study of PV properties, the two-layer ITO/ZnPc(40 nm)/C_{60}(40 nm)/Al and three-layer ITO/ZnPc(40 nm)/C_{60}(40 nm)/BCP(10 nm)/Al cells with variously modified ITOs were fabricated by using a vapor deposition system, as illustrated in **Fig. 2.1.** All the materials were deposited using vacuum evaporation under a pressure of 5-7×10^{-6} Torr at deposition rates of 1-1.5 Å/s for organic layers and 3-4 Å/s for Al cathode. The film thickness of each layer was monitored by a quartz crystal microbalance with a CRTM 8000 controller (ULVAC Techno. Ltd.) placed in the same height as the ITO substrate. The active area for all the cells was defined to be 5×5 mm^2 by using a shadow mask.

2.2.5. Analytic tools

The current density-voltage (J-V_{bias}) curves were measured under illumination of a simulated solar light with 100 mW cm^{-2} (AM 1.5G) by a solar simulator (Yamashita Denso, YSS-50). Electric data were taken using an Advantest R6145 DC voltage current source unit at room temperature in ambient atmosphere.

2. 3. Results and Discussion

Proposed energy level diagrams [29] for the organic PV cells used this study are shown in **Fig. 2.2.** In our previous study, the contact potential difference (CPD) values observed against a gold atomic force microscope tip modified with 1-decanethiol [18,30] were measured for four kinds of ITO electrodes: *i*) treated in air at 120^0C after the cleaning, *ii*) as-cleaned, *iii*) modified of with H- and *iv*) Cl-terminated benzenesulfonyl chlorides. After words, calculated CPDs of as-cleaned ITO and ITO modified with H- and Cl-terminated benzenesulfonyl chlorides with respect to ITO treated at 120^0C for 1 h after the cleaning are ~ –150, –280 and –490 mV, respectively. The effective work functions of variously modified ITO in **Fig. 2.2**

were estimated from the CPD values calculated above together with the assumption that the work function of ITO treated at 120^0C after cleaning agrees with the consistent value of 4.5±0.1 eV for the work function of as-received bare ITO [31,32].

Two kinds of self-assembly molecules, H-and Cl-terminated benzenesulfonyl chlorides have a high electron affinity for -OH groups due to chemisorptions of the molecule onto the ITO substrate. The molecules also show varying degrees of electron-withdrawing character, resulting in different magnitude of dipole moment. In this case, the result is a large dipole moment, μ, pointing towards the ITO surface and it has been shown to result in an increased work function of the ITO surface [4]. The effective work functions of ITO were calculated from the CPD values for the ITO modifiers such as 4.78 eV for H- and 4.99 eV for Cl-terminated benzensulfonyl chlorides [18,29].

Fig. 2.3 shows the J-V_{bias} characteristics of ITO(as-cleaned)/ZnPc(40 nm)/C_{60}(40 nm) cells under white light illumination of 100 mW cm^{-2} in organic PV cells with and without BCP. The PV characteristics are obtained in a two-layer cell with 40 nm and 40 nm layer thickness for ZnPc and C_{60}, respectively, (see **Fig. 2.3**): under illumination the V_{oc} was 0.30 V, the J_{sc} = 1.96 mA cm^{-2}, the FF = 0.22 and the η_p = 0.13 %. The V_{oc} of a three-layer cell (**Fig. 2.2(b)**) was 0.49 V higher than for two-layer cell (**Fig. 2.2(a)**), although both J_{sc} and FF were improved, resulting in an increased the η_p. In this case, FF (0.38) of the cell with BCP was 1.7 times higher than that of the cell without BCP (0.22), accompanied by a nearly 30 % increase in J_{sc}. Generally, the cells with BCP show a much better behavior with respect to the two-layer structure cells.

The J-V_{bias} characteristics of ITO/ZnPc(40 nm)/C_{60}(40 nm)/ BCP(10 nm)/Al cells with ITO electrodes with different WFs are shown in **Fig. 2.4**, and their PV characteristics are summarized in **Table 2.1**. The results show that the ITO modified by H- and Cl-terminated

benzenesulfonyl chloride should be better improved the PV characteristics by providing a good contact with ZnPc. In fact, the chemical modification of ITO by SAM with a dipole moment of appropriate direction and magnitude was an effective way to change the work function of ITO and to decrease the energy barrier or step between ITO and the highest occupied molecular orbital (HOMO) level of ZnPc as an electron donor in organic PV cells.

In the cell with chemically modified with H-terminated benzenesulfonyl chlorides, the PV performance improve significantly, such as the J_{sc}, V_{oc}, *FF*, and η_p were measured 2.70 mA cm^{-2}, 0.53 V, 0.51, and 0.75 %, respectively, as shown in **Table 2.1.** This result suggested that the WF of ITO modified with H-terminated benzenesulfonyl chloride is shifted down to the HOMO level of ZnPc resulting in formation of ohmic contact at the ITO/ZnPc. interface. In the case of cell with as-cleaned ITO anode showed relatively poorer performance to compare with ITO modified with H- and Cl-terminated benzenesulfonyl chlorides. The PV performance of organic PV cells with chemically modified ITO was correlated with the WF change, are improved by the chemical modification of ITO [26].

Conclusion

We have examined the PV characteristics of the organic PV cells using the ZnPc/C_{60} heterojunction layer under 100 mW cm^{-2} illumination of white light source. We have fabricated two types of device structures to see the effect of BCP as the electron transport layer. One is ITO/ZnPc/C_{60}/Al and the other is ITO/ZnPc/C_{60}/BCP/Al. The organic PV cells with BCP have more than 1.7 times the *FF* as compared to typical two-layer devices without BCP, resulting in a more than 3.6 times of the η_P. Moreover, PV performance was increased significantly by using chemically modified ITO electrodes with SAM. This study supports the

device performance that change in WF of ITO and introduction of BCP thin layer between C_{60} and Al interface are dominate factors in improving PV characteristics in organic PV cells.

Chemically modified ITO electrodes with SAM with a dipole moment of appropriate direction and magnitude was an effective way to change the WF of ITO and to decrease the injection barrier between ITO and the HOMO level of ZnPc as an electron donor in organic PV cells. In addition, the WF of chemically modified ITO with SAM treated by H-terminated benzenesulfonyl chloride was shifted down to HOMO level of ZnPc, which results the ohmic contact at the ITO/ZnPc interface.

References

1. R. W. Murray, in Electroanalytical Chemistry, **13**, edited by A. J. Bard, (Marcel Dekker, New York), p. 191-368 (1984).
2. Fujihira M. in Topics in Organic Electrochemistry, edited by A. J. Fry and W. E. Britton, (Plenum, New York), p. 255-294 (1986).
3. R. Murray. **22**, Techniques of Chemistry, (John Wiley & Sons, New York), p. 1-48. (1992).
4. Ganzorig C, Fujihira M, in "Chemically Modified Oxide Electrodes", "Modified Electrodes" edited by A. J. Bard and M. Stratmann, Encyclopedia of Electrochemistry, Vol. **10**, WILEY-VCH Verlag GmbH, Weinheim, p. 261-334 (2007).
5. C.W. Tang, Appl. Phys. Lett. **48**, 183 (1986).
6. C.W. Tang, S.A. Van Slyke, Appl. Phys. Lett., **51**, 913 (1987).
7. M. Fujihira and C. Ganzori, in Conjugated Polymer and Molecular Interfaces, edited by A. Kahn, J. J. Pireaux, W. R. Salaneck, and K. Seki, (Marcel Dekker, New York), 817-858 (2002).
8. M. Fujihira, N. Ohishi, and T. Osa, Nature (London). **268**, 226 (1977).
9. M. Fujihira, T. Kubota, and T. Osa, J. Electroanal. Chem. **119**, 379 (1981).
10. T. J. Gardner, C. D. Frisbie, and M. S. Wrighton, J. Am. Chem. Soc. **117**, 6927 (1995).
11. F. Nűesch, L. Si-Ahmed, B. Francois, and L. Zuppiroli, Adv. Mater. **9**, 222 (1997).
12. F. Nűesch, F. Rotzinger, L. Si-Ahmed, and L. Zuppiroli, Chem. Phys. Lett. **288**, 861 (1998).
13. L. Zuppiroli, L. Si-Ahmed, K. Kamaras, F. Nűesch, M. N. Bussac, D. Ades, A. Siove, E. Moons, and M. Grätzel, Eur. Phys. J. B. **11**, 505 (1999).
14. F. Nűesch, M. Carrara, and L. Zuppiroli, Langmuir. **19**, 4871 (2003).

15. S. G. Conto, M. Carrard, L. Si-Ahmed, and L. Zuppiroli, Adv. Mater. **11**, 112 (1999).
16. S. F. J. Appleyard and M. R. Willis, Opt. Mater. **9**, 120 (1998).
17. S. F. J. Appleyard, S. R. Day, R. D. Pickford, and M. R. Willis, J. Mater. Chem. **10**, 169 (2002).
18. C. Ganzorig, K. J. Kwak, K. Yagi, and M. Fujihira, Appl. Phys. Lett. 79, 272 (2001).
19. Y. Enatsu, C. Ganzorig, and M. Fujihira, Mat. Res. Soc. Sym. Proc. **771**, 111 (2003).
20. C. Ganzorig, M. Sakomura, K. Ueda, and M. Fujihira, Appl. Phys. Lett. **89**, 263501 (2006).
21. C. Ganzorig and M. Fujihira, "Study of Hole Injection in Hole-Only Single-Carrier Devices", "Multifuntional Conducting Molecular Materials" edited by G. Saito, F. Wudl, R. C. Haddon, K. Tanigaki, T. Enoki, H. E. Katz, and M. Maesato, RSCPublishing, Royal Society of Chemistry, p. 253-269 (2007).
22. J. Morgado, A. Charas, and N. Barbagallo, Appl. Phys. Lett. **81**, 933 (2002).
23. J. Morgado, N. Barbagallo, A. Charas, M. Matos, L. Alcacer, and F. Cacialli, J. Phys. D. Appl. Phys. **36**, 434 (2003).
24. J. Morgado, N. Barbagallo, V. Bodrozic, A. Teixeira, A. C. Fernandes, R. Guntner, U. Scherf, F. Cacialli, and L. Alcacer, Synth. Met. **154**, 153 (2005).
25. S. Khodabakhsh, D. Poplavskyy, S. Heutz, J. Nelson, D. D. C. Bradley, H. Murata, and T. S. Jones, Adv. Funct. Mater. **14**, 1205 (2004).
26. S. Khodabakhsh, B. M. Sanderson, J. Nelson, and T. S. Jones, Adv. Funct. Mater. **16**, 95 (2006).
27. C. Donley, D. Dunphy, D. Paine, C. Carter, C. Nebesny, P. Lee, D. Alloway, and N. R. Armstrong: Langmuir. **18**, 450 (2002).

28. N. R. Armstrong, C. Carter, C. Donley, A. Simmonds, P. Lee, M. Brumbach, B. Kippelen, B. Domercq, and S. Yoo, Thin Solid Films. **445**, 342 (2003).
29. K. Sarangerel, C. Ganzorig, M. Fujihira, M. Sakomura, and K. Ueda, "Influence of the Work Function of Chemically Modified Indium–Tin Oxide Electrodes on the Open-Circuit Voltage of Heterojunction Photovoltaic Cells," Chem. Lett., **37**, pp. 778 (2008).
30. M. Fujihira, Annu. Rev. Mater. Sci. **29**, 353 (1999).
31. J. S. Kim, M. Granstrom, R. H. Friend, N. Johansson, W. R. Salaneck, R. Daik, W. J. Feast, and F. Cacialli, J. Appl. Phys. **84**, 6859 (1998).
32. K. Sugiyama, H. Ishii, Y. Ouchi, and K. Seki, J. Appl. Phys. **87**, 295 (2000).

Tables and Figures

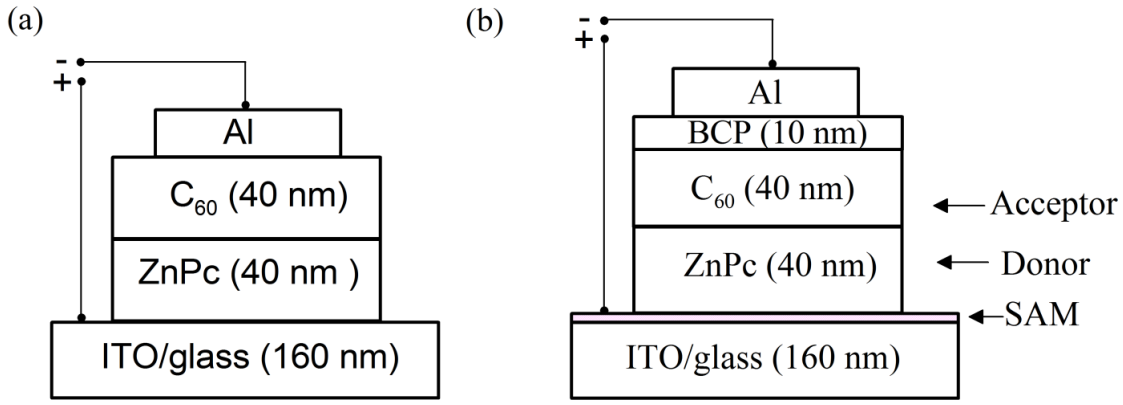

Fig. 2.1. Device structures of (a) two-layer ITO/ZnPc(40 nm)/C_{60}(40 nm)/Al and (b) three-layer ITO (SAM)/ZnPc(40 nm)/C_{60}(40 nm)/BCP(10 nm)/Al cells.

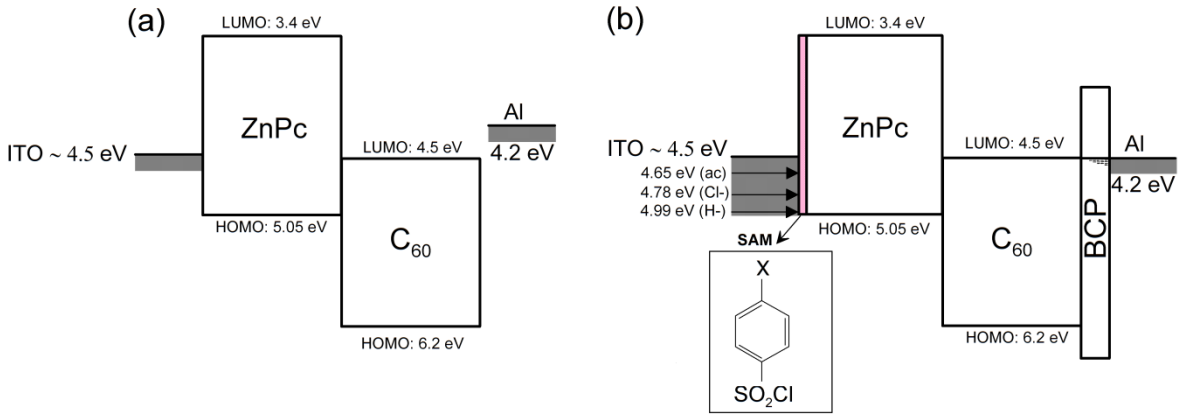

Fig. 2.2. Schematic energy diagrams for (a) two-layer and (b) with BCP layer organic PV cells.

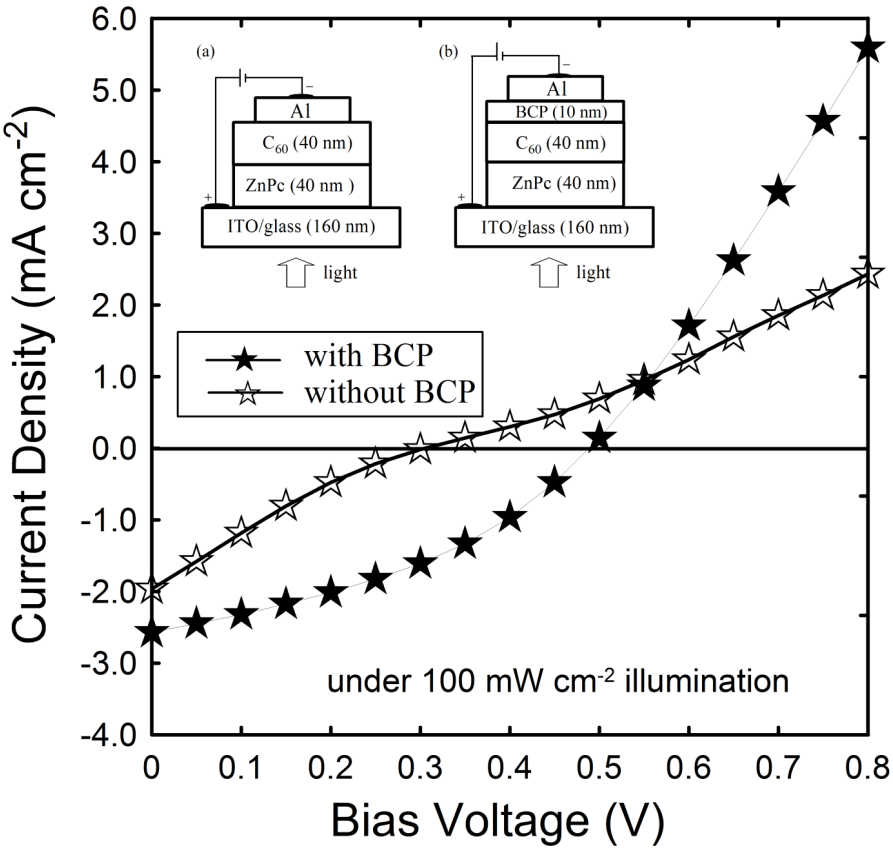

Fig. 2.3. *J*-V_{bias} characteristics of organic PV cells on "as-cleaned" ITO with and without BCP as an exciton blocking layer under 100 mW cm^{-2} illumination.

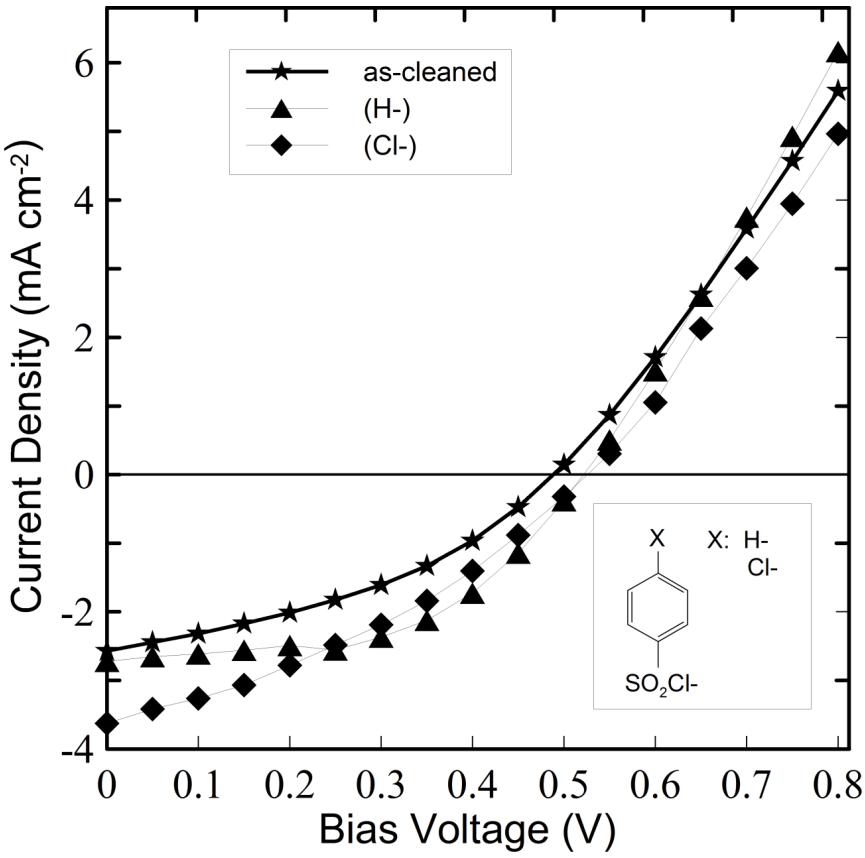

Fig. 2.4. The J-V_{bias} characteristics of ITO/ZnPc(40 nm)/C_{60}(40 nm)/BCP(10 nm)/Al cells with different treated ITO electrodes as-cleaned and chemically modified with H- and Cl-terminated benzensulfonyl chlorides under 100 mW cm^{-2} illumination.

Table 2.1 Photovoltaic characteristics for the organic PV cells using ITO chemically modified with H- and Cl-terminated benzensulfonyl chlorides under 100 mw cm^{-2} illumination.

	Modified ITO	J_{sc} (mA/cm^2)	V_{oc} (V)	*FF*	η_p (%)
Without BCP	*(as-cleaned)*	1.96	0.30	0.22	0.13
With BCP	*(as-cleaned)*	2.56	0.49	0.38	0.48
	H-terminal	2.70	0.53	0.51	0.75
	Cl-terminal	3.60	0.53	0.34	0.66

Chapter 3

Detailed Investigation of Dependencies of Photovoltaic Performances of P3HT:PC61BM based Solar Cells on Anodic Work Function Modified by Surface Treatment of ITO Electrode with Benzenesulfonyl Chloride Derivatives

3.1. Introduction

Indium-tin-oxide (ITO) is one of the most widely used materials for transparent electrodes in organic electronic devices, e.g., organic electroluminescent diodes (OELDs) [1], polymer light emitting diodes [2], and organic photovoltaic (PV) cells [3], because of its high electrical conductivity and optical transparency in the visible spectral range. However, the work function (WF) of ITO is generally not high enough to achieve Ohmic contact with a layer of organic electronic material. Therefore, there is a barrier when hole injection from ITO to an organic material takes place. Thus, various surface treatments such as UV-ozone treatment [4], the spin-coating of a poly(3,4-ethylenedioxythiophene):poly(styrene sulfonate) (PEDOT:PSS) film [5,6], and the self-assembly of a monolayer of dipolar molecules [7–10] on an ITO substrate have been attempted to change the WF of ITO in order to reduce the hole injection barrier height [11]. In our previous study, the characteristics of OELDs based on N,N'-diphenyl-N,N'-bis(3-methylphenyl)-1,1'-biphenyl-4,4'-diamine (TPD) /tris(8-hydroxyqunoline) aluminum (Alq_3) were dramatically improved using self-assembled monolayer (SAM) modification of the ITO surface with dipolar-molecules of H-, Cl-, and CF_3-terminated benzoyl chlorides. The barrier height for the hole injection from the Cl-terminated SAM-modified ITO to TPD was estimated to be as small as 0.095 eV, using a calculation based on the Fowler–Nordheim tunneling theory [9].

Like other organic electronic devices, charge injection at the ITO/organic layer interface

is a key issue for organic PV cells [12,13]. Khodabakhsh *et al.* [8] reported the use of a series of SAMs based on conjugated molecular species as a means to control the wettability and WF of the ITO anode of copper phthalocyanine (CuPc)/fullerene (C_{60})-based small-molecule organic PV cells. In their study, the WF of SAM-modified ITO was successfully controlled within a range of 4.9−5.1 eV using three self-assembly molecules. They observed an improved efficiency and a larger short-circuit current density (J_{sc}) for organic PV cells using ITO electrodes modified by dipolar-molecule SAMs compared to untreated ITO. However, the values of open-circuit voltage (V_{oc}) did not change when using the SAM-treated ITOs, compared to the untreated ITOs. Such insensitivity of V_{oc} to the variation in the WF of the SAM-modified ITO of pentacene (PEN)/C_{60}-based organic PV cells was also reported by Sharma *et al.* [14]. They correlated it with an invariance of the charge injection barrier due to Fermi level pinning at the ITO/PEN interface.

It has been suggested that the V_{oc} values in organic PV cells depend either on the difference in the energies between the HOMO of the donor and lowest occupied molecular orbital (LUMO) of the acceptor or the WF difference ($\Delta\phi$) between the electron-collecting (EC) and hole-collecting (HC) electrodes [15–17]. Using large WF values for the ITOs used as HC electrodes, an improvement in the built-in potential (V_{bi}) resulting from $\Delta\phi$ would be expected with organic PV cells. The enhancement of V_{bi} contributes to an improvement in the efficiency of the charge separation and transport away from the donor-acceptor heterojunction interface. As commonly indicated in the literature on organic PV cells, in which V_{bi} is estimated by measuring V_{oc} for various incident light intensities, V_{oc} has direct dependence on V_{bi} [18,19].

In our attempt to understand the origin of V_{oc} for organic PV cells, we previously investigated the effect of modifying the ITO WF with dipolar-molecule SAMs on the device

performances of small molecule organic PV cells with ITO/donor/C_{60}/bathocuproine (BCP)/Al by employing three kinds of donors: zinc phthalocyanine (ZnPc), rubrene (Rub), and boron subphthalocyanine chloride (SubPc) [16]. With an increase in the anode WF of the Rub/C_{60}-based and SubPc/C_{60}-based organic PV cells in a range of approximately 4.6 to 5.0 eV, V_{oc} increased almost linearly (approximately unit slope) from approximately 0.5 to 0.9 V. It then saturated and became constant at approximately 0.9 V at the higher $\Delta\phi$ region from approximately 5.0 to 5.3 eV. The two distinct regions with the different V_{oc} dependences, "linear" and "constant," seem to correspond to non-ohmic and ohmic contacts, respectively. In the case of the former contact, the experimental V_{oc} is in agreement with the $\Delta\phi$ of the EC and HC electrodes, whereas the latter results in Fermi level pinning [15].

Knesting *et al.* [20] reported a similar V_{oc} dependence characterized by linear and saturated regions in a recent study on the effect of dipolar SAMs on the V_{oc} and recombination kinetics in polymer/fullerene bulk hetero-junction (BHJ) organic PV cells. By employing three kinds of phosphonic acid compounds, they obtained three kinds of SAM-modified ITOs with different WFs (approximately 4.2, 4.5, and 5.1 eV) and used them to fabricate two series of BHJ organic PV cells with the following structures: ITO/SAM/super yellow (SY)/[6,6]-phenyl-C_{71}-butyric acid methyl ester ($PC_{71}BM$)/LiF/Al and ITO/SAM/poly(3-hexylthiophene) (P3HT)/[6,6]-phenyl-C_{61}-butyric acid methyl ester ($PC_{61}BM$)/LiF/Al. A linear dependence of V_{oc} on the anode WF was observed with SY/$PC_{71}BM$-based organic PV cells, whereas a saturation region appeared with P3HT:$PC_{61}BM$-based organic PV cells. As for P3HT:$PC_{61}BM$-based BHJ organic PV cells, an early study by Kim *et al*. [21] investigated the effect of SAM-treated ITOs with different WFs: 3.87, 4.35, and 5.16 eV. However, the effect of modifying the WF of the ITO with dipolar-molecule SAMs on the device performances of BHJ organic PV cells has not been sufficiently characterized.

In particular, a detailed investigation of the changes in the device performances resulting from systematic changes in the anode WF at a potential range near the HOMO level of the donor is important to design efficient BHJ organic PV cells.

In this chapter, we attempted to improve the PV characteristics of P3HT:$PC_{61}BM$-based BHJ organic PV cells using ITO electrodes chemically modified with CH_3O-, H-, Cl-, CF_3-, and NO_2-terminated benzenesulfonyl chlorides as the SAM. We examined the correlation between the ITO WFs corrected by the change in the contact potential difference (CPD) and the calculated dipole moments of SAM models. We found that the fine-tuning of the ITO WF within a range up to ~0.6 eV higher than a non-treated ITO WF could be realized by the SAM modification with the different terminal groups of *p*-benzenesulfonyl chloride. In contrast to the former studies by other groups [20,21], in which the SAM modification of ITO by three dipolar molecules provided only one kind of modified WF lying near the HOMO energy level of P3HT, we examined the PV characteristics of P3HT:$PC_{61}BM$ based BHJ organic PV cells using five types of SAM-modified ITOs with different WFs lying within ±0.20 eV from the HOMO energy level of P3HT. In order to develop an optimized contact at the ITO/P3HT interface, a detailed investigation and discussion focusing on the range of WFs close to the HOMO energy of P3HT would be required.

3.2. Experimental

3.2.1. Materials

Organic semiconductor materials such as P3HT and $PC_{61}BM$ are known to be stable during spin-coating deposition in a glove box. P3HT and $PC_{61}BM$ were purchased from Luminescence Technology Corp. and Frontier Carbon Corp., respectively, and used without further purification. BCP and PEDOT:PSS were purchased from Tokyo Chemical Industry

and Heraeus, respectively, and used as charge-collecting buffer layers. All the other solvents and reagents used were of analytical grade and purchased commercially. Anhydrous solvents were used during the chemical modification.

3.2.2. Substrate preparation

The substrates used in this study were 160-nm-thick ITO-coated glass plates with a resistance of approximately 15 Ω/square supplied by Sanyo Vacuum Industries. The substrates were cut into 10 × 12 mm^2 sample slides, and the ITO layers were etched using an aqua regia solution to form 2-mm-wide stripes for use as anodes. The patterned ITO substrates were cleaned and rinsed using two detergent solutions (Extran MA 03, pH 6.8, MERCK and Kontaminon O, pH 10, WAKO) and deionized water, and then stored under isopropanol until required. Prior to use, the ITO substrates were further cleaned, successively ultrasonicated in acetone and isopropanol, and then transferred to boiled isopropanol. This cleaned ITO will hereafter be called the "as-cleaned ITO."

3.2.3. Chemical modification of ITO electrode

Schematic drawings of the formation of monolayers by self-assembly at ITO electrode surfaces were given in previous studies [9,16]. After cleaning, the ITO substrates were immersed for 10 min in dichloromethane solutions containing 1 mM of *p*-substituted benzenesulfonyl chloride (Tokyo Chemical Industry) to form the SAM-modified ITO [11,22–24]. The modified ITO electrodes were rinsed in pure dichloromethane to remove excess unbound molecules and then dried in a glove box. The change in the WF due to the surface modification of the ITO was observed by Kelvin probe force microscopy (KFM) [25–28] using a gold-coated atomic force microscopy (AFM) tip. For comparison, the as-cleaned ITO without chemical modification was also used for the measurement of the WF by KFM.

3.2.4. Device fabrication and characterization

A polymer blend (P3HT:$PC_{61}BM$) solar device configuration with P3HT as the *p*-type donor and $PC_{61}BM$ as the *n*-type acceptor in a photo-active layer is illustrated **in Fig. 3.1.** A solution with a 1:0.8 weight ratio of P3HT to $PC_{61}BM$ was prepared in dichlorobenzene (17 g/L) and then stirred well using ultrasonication for over 2.5 h. After spin coating (900 rpm) the photo-active layer (~150 nm) prepared from the P3HT:$PC_{61}BM$ solution on the ITO electrodes with and without the surface modification by the *p*-benzenesulfonyl chlorides with different terminal groups (see **Fig. 3.1**), the blend film was dried at 110°C for 10 min in the glove box. Then, the BCP (5 nm) layer and Al (~100 nm) cathode were deposited using thermal evaporation in a vacuum chamber (~2-5 × 10^{-4} Pa) with deposition rates of ~1.0–1.5 and 2–5 Å s^{-1}, respectively, on all the organic PV cells. For comparison, ITO spin-coated with the conventional PEDOT:PSS hole-collecting layer was used for the device configuration. The PEDOT:PSS film (~100 nm) coated on the ITO was also dried at 100°C for 10 min. The film thicknesses for the spin-coated P3HT:$PC_{61}BM$ and PEDOT:PSS films were found to be ~150 nm and ~100 nm, respectively, using the AFM [29].

The photo-active area was defined as the overlap between the ITO anode and counter Al cathode (2 × 2 mm^2). The thicknesses of the P3HT:$PC_{61}BM$ and PEDOT:PSS layers were controlled by the spin coating parameters. To monitor and control the thicknesses of the BCP and Al layers, a quartz crystal microbalance with a CRTM 6000G controller (ULVAC Techno Ltd.) was placed in the vacuum chamber. The PV characteristics of the cells were measured in the dark and under the illumination of a simulated solar light with 100 mW/cm^2 (AM1.5G) using a solar simulator (Yamashita Denso, YSS-50) in air. Electric data were obtained using an Advantest R6145 DC voltage current source unit at room temperature in the ambient atmosphere.

3.2.5. Calculation

The dipole moments of the surface-active organic molecules were calculated using the *ab* initio method. The geometries of the molecules were optimized using the density functional theory (DFT) with Becke`s three-parameter hybrid exchange functional [30], the Lee–Yang–Parr correlation functional (B3LYP) [31], and the 6-311+G(d,p) basis set [32] method implemented in the Gaussian 03 package [33]. Then, the dipole moments along the first principal axis of the molecules were evaluated. The molecules were *p*-benzenesulfonyl chlorides with the CH_3O-, H-, Cl-, CF_3-, and NO_2-terminal groups, and the first principal axis of these molecules corresponded to the direction normal to the surface (μ_{per}) of the SAM model, as shown in Fig. 3.1.

3.3. Results and discussion

3.3.1. Work function of SAM-modified ITO electrode

The WFs could be changed by the adsorption of SAM molecules on the ITO surface. In order to elucidate the WF change of the ITO with the SAM-modified surface, KFM measurements were performed using highly oriented pyrolytic graphite (HOPG) as the standard reference surface (WF of 4.475 eV). The CPD values were obtained for the HOPG surface, as-cleaned ITO, PEDOT:PSS coated ITO and SAM-modified ITOs with the CH_3O-, H-, Cl-, CF_3-, and NO_2-terminal groups of *p*-benzenesulfonyl chloride. The CPD values were measured against the gold AFM tip [34]. The expected differences in WFs between the modified ITOs with the CH_3O-, H-, Cl-, CF_3-, and NO_2-terminal groups and the HOPG surface were estimated from the differences in the corresponding CPD values (ΔV_{CPD}). **Table 3.1** lists the values of ΔV_{CPD} and the corrected WFs compared to the HOPG surface. In the

same manner, the corrected WFs of the as-cleaned ITO and the PEDOT:PSS coated ITO were estimated to be ~4.73 and ~5.20 eV, respectively.

The calculated dipole moments of μ_{per} for the molecules of the *p*-benzenesulfonyl chlorides with the CH_3O-, H-, Cl-, CF_3-, and NO_2-terminal groups are also listed in **Table 3.1.** The relation between the WFs of the modified ITO and the calculated dipole moments is shown in **Fig. 3.2**. An almost linear relationship can be observed, where the WF decreases with an increase in the dipole moment of the SAM molecules [7,35–38].

The substitution of benzoic acid in the *para* position with moieties having varying electron-withdrawing or -donating properties is well known to alter the WF [39–41]. Khodabakhsh *et al*. observed a linear trend between the WF and calculated dipole moments of *p*-substituted benzene derivatives with different binding groups [8]. Hotchkiss *et al*. obtained a similar linear correlation between the WF and dipole moments of benzylphosphonic acid derivative molecules [42]. Our experimental results also showed a similar linear correlation in the case of the series of benzenesulfonyl chlorides.

3.3.2. Dark current density–voltage characteristics of BHJ PV cells

The dark current density–voltage (J–V_{bias}) characteristics of our BHJ PV cells with various SAMs modified ITOs, as well as the as-cleaned ITO and PEDOT:PSS-coated ITO, are shown in **Fig. 3.3.** The dark current density, J_D, at a given voltage increases in the order J_D(as-cleaned ITO) ≈ $J_D(CH_3O) < J_D$(H) < J_D(PEDOT:PSS) < J_D(Cl) < $J_D(CF_3) < J_D(NO_2)$. In the results for the SAM-modified ITOs, the dark current density increases with an increase in the anode WF. This result can be explained in terms of the modification of the interfacial hole injection barrier or step, which is defined as the difference between the HOMO energy of the donor and the anode WF [8]. The WF value of the PEDOT:PSS-coated ITO is exceptionally high compared to that of the Cl-terminated benzenesulfonyl chloride-modified ITO, in spite

of a lower current density. PEDOT:PSS has a heterogeneous structure, in which small conductive grains are separated by regions rich in insulating PSS [6,42]. If the conductivity mechanism of such a heterogeneous material reduces the effective area of the contact contributing to ohmic injection, there will be an apparent reduction in the plotted J_D for PEDOT:PSS in Fig. 3.3, where the values of J_D were calculated by assuming that the whole device area was responsible for injection [43].

3.3.3. Photovoltaic properties with SAM-modified ITOs

Fig. 3.4(a) shows the J–V_{bias} characteristics of all the prepared cells under simulated AM 1.5 illumination. For all the devices of the SAMs or PEDOT:PSS-treated ITOs, an almost constant V_{oc} around 0.6 V, which was approximately 0.1 V larger than that of the as-cleaned ITO device, was observed, as shown in the upper part of **Fig. 3.4(b).** Such V_{oc} saturation is similar to the result reported by Knesting *et al.* [20]. In the present case, the WF values of all five SAM-modified ITOs and of PEDOT:PSS lie within ±0.2 eV from the HOMO energy level of the P3HT donor (5.1 eV). The corresponding interfacial energy gap or step to the energy difference between the modified WFs and the HOMO of the donor seems to be small enough for approximately ohmic charge injection. Therefore, the saturation of V_{oc} is to be expected [8,44].

The observed device performances of J_{sc}, V_{oc}, FF, and the power-conversion efficiency (η_P) are summarized in **Table 3.2.** The effect of the SAM modification on J_{sc} and FF is remarkable, with J_{sc} increasing from 7.88 mA cm^{-2} (for the as-cleaned ITO) to 12.82 mA cm^{-2} (for the Cl-treated ITO), and FF increasing from 0.33 (for the as-cleaned ITO) to 0.54 (for the NO_2-treated ITO). As a result of these improvements, the enhancement effect of the SAMs on

η_P reached its maximum with Cl (η_P = 3.72%), and became larger than that of PEDOT:PSS (η_P = 3.62%).

The dependence of J_{sc} on the anode WF is shown in the lower part of **Fig. 3.4(b).** It is somewhat complicated. Therefore, we will consider two WF regions for the modified ITO to obtain better insight. One WF region is lower and the other is higher than the energy of the HOMO level of the P3HT used as the donor. The WF of the Cl-modified ITO nearly coincides with the HOMO energy of the donor. Therefore, Cl belongs to both regions.

First, in the region of the lower anode WF, J_{sc} increases in the order J_{sc}(as-cleaned ITO) < $J_{sc}(CH_3O) < J_{sc}$(H) < J_{sc}(PEDOT:PSS) < J_{sc}(Cl), This is the same order as observed for the J_D measurements, in which the current increased with an increase in the anode WF, with the exception of PEDOT:PSS, which resulted in a lower current than Cl, in spite of its higher WF. As assumed in the above discussion on J_D, the reduced J_{sc} of PEDOT:PSS was likely a consequence of the heterogeneous hole injection, which was possibly the mechanism responsible for reducing the effective area of contact.

In general, the improved built-in potential that results from the increase in $\Delta\phi$ would be expected to increase V_{oc} and J_{sc} through the increased electric field at short circuit [45]. However, the J_{sc} results for the SAM-modified anodes, except for the PEDOT:PSS-modified anode result, showed a monotonic increase with an increase in the WF, without significant variation in V_{oc}. Such dependence of J_{sc} on the WF suggests that the current flow would be affected by some underlying mechanism related to the anode WF. One of the possible explanations for such J_{sc} dependence is given by the presence of band-bending at the anode-conjugated polymer interface [46]. When the Fermi level pinning position at an anode-polymer interface is limited by the energy level of the interface's positive polaron P^+,

downward (positive) band bending in the polymer layer would be exhibited by the integer charge transfer (ICT) mechanism [47]. The P^+ state can be regarded as a positively charged state stabilized by the extra polarization from the electrode, and thus is expected to lie within the band gap [48]. In the ICT model, a hole layer near the polymer-electrode interface is created by hole transfer from the electrode to the polymer when the WF of the electrode becomes larger than the energy level of the P^+ state. The depth of the band-bending increases with an increase in the anode WF. Because the field of the band-bending region can accelerate the hole transport toward the HC electrode, an increase in the anode WF might improve the yield of the hole correction on the ITO anode of the device [51].

Zhang *et al.* reported Fermi level pinning for a P3HT/PEDOT:PSS-coated ITO interface determined by the P3HT polaronic level P^+, which was observed to be 0.2 eV lower than the HOMO level of P3HT [46]. Accordingly, the present result of V_{oc} saturation observed at the lower WF of 4.90 eV (for the CH_3O-treated ITO), which was 0.2 eV lower than the P3HT HOMO level, was probably due to the Fermi level pinning to the P^+ level. Taking into account the reduction of the built-in potential due to the downward band bending of 0.2 eV, the observed V_{oc} of around 0.6 eV corresponded well with the value expected from the difference between P3HT HOMO (5.1 eV) and $PC_{61}BM$ LUMO (4.3 eV).

In contrast to the lower WF region, the reverse dependence of J_{sc} is displayed in the second region of the higher WF, i.e., J_{sc} decreases with an increase in the anode WF. Although the maximum WF of 5.28 eV (for the NO_2-treated ITO) resulted in a higher J_D (NO_2), the J_{sc} (NO_2) of 8.62 mA cm^{-2} was even lower than the J_{sc} (PEDOT:PSS) of 9.43 mA cm^{-2} and J_{sc} (H) of 8.94 mA cm^{-2}. On the other hand, the V_{oc} saturation was continuously displayed over the higher WF region. This result suggests that a similar pinning position was also reproduced with the CF_3- and NO_2-treated ITOs. It should be noted that, in the higher

WF region, the energy level alignment at the P3HT/ITO interface was achieved, not only by hole transfer from the anode to the polymer P^+ level, as in the case of the lower WFs, but also by electron transfer from the polymer HOMO band to the anode. When an electron transfers from the HOMO band, it creates a hole in P3HT. The electric double layer at the P3HT-ITO junction caused by the electron transfer led to a discontinuous jump in the electrostatic potential at the junction, which reduced the contribution of the band bending to the compensation of the potential difference between the anode WF and the P^+ level [51]. The change from the positive to negative dependence of J_{sc} on the anode WF may be correlated to the change in the method for achieving the energy level alignment at the P3HT/ITO interface. Furthermore, it is known that even slight oxidation of the conjugated polymer may yield a dramatically higher dark conductivity and results in an additional non-photo-induced current [49,50]. This factor leads to the reduction of the device performance, and thus possibly explains the decrease in J_{sc} observed with the anode WF, which lies beyond the oxidation potential of P3HT.

Conclusion

We correlated the changes in the WF of SAM-modified ITO with the calculated dipole moments of SAM models and the PV performances of P3HT:PC_{61}BM-based organic cells. An almost linear relationship was observed between the values of the ITO WF determined by KFM measurements and the calculated dipole moments of μ_{per} for p-benzenesulfonyl chloride molecules with the CH_3O-, H-, Cl-, CF_3-, and NO_2-terminal groups. Based on a detailed investigation using ITO WFs lying within ±0.2 eV from the P3HT HOMO level (5.1 eV), two distinct J_{sc} dependencies, i.e., increasing and decreasing with an increase in the WF of the anode ITO, were observed for WFs higher and lower than the HOMO level of the donor, respectively. Consequently, the enhancement effect of the SAM on η_P reached its maximum

(η_P = 3.72%) at a WF of 5.11 eV (for the Cl-treated ITO). In contrast to the J_{sc} dependencies, almost the same V_{oc} values (around 0.6 V) were observed with the different SAM-modified ITOs. The constant V_{oc} observed even at a WF of 4.90 eV (for the CH_3O-treated ITO), which was 0.2 eV lower than the P3HT HOMO level, suggested that Fermi level pinning was achieved by aligning the anode Fermi level and positive polaronic level of the donor polymer [51]. The V_{oc} value of the P3HT:$PC_{61}BM$-based PV cell corresponded well to the difference between the polaronic level, which was assumed to be 0.2 eV lower than the HOMO level of P3HT, and the LUMO level of $PC_{61}BM$ (4.3 eV).

References

1. C. W. Tang, S. A. VanSlyke, Appl. Phys. Lett. **51**, 913 (1987).
2. I. D. Parker, Appl. Phys. Lett. **75**, 1656 (1994).
3. C. W. Tang, Appl. Phys. Lett. **48**, 183 (1986).
4. S. Y. Kim, J.-L. Lee, K.-B. Kim, Y.-H. Tak, J. Appl. Phys. **95**, 2560 (2004).
5. T. M. Brown, J. S. Kim, R. H. Friend, F. Cacialli, R. Daik, W. J. Feast, Synth. Met. 111-112, 285 (2000).
6. M. M. de Kok, M. Buechel, S. I. E. Vulto, P. van der Weijer, E. A. Meulenkamp, S. H. P. M. de Winter, A. J. G. Mank, H. J. M. Vorstenbosch, C. H. L. Weijtens, V. van Elsbergen, Phys. Stat. Sol. (a) **201**, 1342 (2004).
7. C. Ganzorig, K. Kwak, K. Yagi, M. Fujihira, Appl. Phys. Lett. **79**, 272 (2001).
8. S. Khodabakhsh, B. M. Sanderson, J. Nelson, T. S. Jones, Adv. Funct. Mater. **16**, 95 (2006).
9. C. Ganzorig, M. Sakomura, K. Ueda, M. Fujihira, Appl. Phys. Lett. **89**, 263501(2006).
10. S. F. J. Appleyard, S. R. Day, R. D. Pickford, M. R. Willis, J. Mater. Chem. **10**, 169 (2000).
11. M. Fujihira, C. Ganzorig, Conjugated Polymer and Molecular Interfaces, eds. by A. Kahn, J. J. Pireaux, W. R. Salaneck, K. Seki (Dekker, New York, 2002) pp.817-858.
12. I. H. Cambell, S. Rubin, T. A. Zawodzinski, J. D. Kress, R. L. Martin, D. L. Smith, N. N. Barashkov, J. P. Ferraris, Phys. Rev. B **54** R14321 (1996).
13. Y. Jang, J. H. Cho, D. H. Kim, Y. D. Park, M. Hwang, K. Cho, Appl. Phys. Lett. **90**, 132104 (2007).
14. A. Sharma, A. Haldi, W. J. Potscavage Jr., P. J. Hotchkiss, S. R. Marder, J. Mater. Chem. **19**, 5298 (2009).

15. V. D. Mihailetchi, P. W. M. Blom, J. C. Hummelen, M. T. Rispens, J. Appl. Phys. **94**, 6849 (2003).
16. K. Sarangerel, C. Ganzorig, M. Fujihira, M. Sakomura, K. Ueda, Chem. Lett. **37**, 778 (2008).
17. C. J. Brabec, A. Cravino, D. Meissner, N. S. Sariciftci, T. Fromherz, M. T. Rispens, L. Sanchez, J. C. Hummelen, Adv. Func. Mater. **11**, 374 (2001).
18. H. Frohne, S. E. Shaheen, C. J. Brabec, D. C. Muller, N. S. Sariciftci, K. Meerholz, Chem. Phys. Phys. Chem. **3**, 795 (2002).
19. P. Kumar, S. C. Jain, H. Kumar, S. Chand, V. Kumar, Appl. Phys. Lett. **94**, 183505 (2009).
20. K. M. Knesting *et al.,* Phys. Chem. Lett. 4, 4038(2013).
21. J. S. Kim, J. H. Park, J. H. Lee, J. D.-Y. Kim, K. Cho, Appl. Phys. Lett. **91**, 112111(2007).
22. C. Ganzorig, M. Fujihira, Encyclopedia of Electrochemistry, Vol **10** Chemically modified oxide electrodes, eds. by M. Fujihira, F. R. James, I. Rubinstein pp.261-343(Wiley-VCH, 2007).
23. M. Fujihira, N. Ohishi, T. Osa, Nature **268**, 226(1977).
24. M. Fujihira, T. Kubota, T. Osa, J .Elecroanal. Chem. **119** 379 (1981).
25. M. Fujihira, H. Kawate, M. Yasutake, Chem. Lett. **21**, 2223(1992).
26. M. Fujihira, H. Kawate, Thin Solid Films **242**, 163 (1994).
27. M. Fujihira, H. Kawate, J. Vac. Sci. Technol. B **12**, 1604 (1994).
28. M. Fujihira, Annu. Rev. Mater. Sci. **29**, 353 (1999).
29. C. Ganzorig, M. Fujihira, Appl. Phys. Lett. **77**, 4211 (2000).
30. A. D. Becke, J. Chem. Phys. **98**, 5648 (1992).
31. C. Lee, W. Yang, R. G. Parr, Phys. Rev. B **37**, 785 (1998).
32. J. R. Cheeseman, G. W. Trucks, T. A. Keith, M. J. Frisch, J. Chem. Phys. **104**, 5497

(1996).

33. J. A. Pople, “Gaussian 03”, Revision C. 01 Gaussian Inc, Wallingford CT, 2004
34. G. G. Malliaras, J. R. Salem, P. J. Brock, C. Scott, Phys. Rev. **B** 58, R13411 (1998).
35. A. Vilan, A. Shanzer, D. Cahen, Nature **404**, 166 (2000).
36. V. Vogel, D. Möbius, J. Colloid Interface Sci.**126**, 408 (1998).
37. R. W. Zehner, B. F. Parsons, R. P. Hsung, P. H. Richard, L. R. Sita, Langmuir **15**, 1121(1999).
38. A. L. McClellan, Tables of Experimental Dipole Moments, Freeman W H and Company, San Francisco (1963).
39. A. L. Swint, P. W. Bohn, Langmuir **20**, 4076 (2004).
40. T. B. McMahon, P. Kebarle, J. Am. Chem. Soc. **99**, 2222 (1977).
41. C. Hansch, A. Leo, R. W. Taft, Chem. Rev. **91**, 165 (1991).
42. P. J. Hotchkiss, L. Hong, P. B. Paramonov, S. A. Paniagua, S. C. Jones, N. R. Armstrong, J. L. Brédas, R. M. Seth, Adv. Mater. **21**, 4496 (2009).
43. E. Vitoratos, S. Sakkopoulos, N. Paliatsas, K. Emmanouil, S. A. Choulis, Open J. Org. Polymer Mater. **2**, 7 (2012).
44. S. Khodabakhsh, D. Poplavskyy, S. Heutz, J. Nelson, D. D. C. Bradley, H. Murata, T. S. Jones, Adv. Func. Mater. **14**, 1205 (2004).
45. J. Nelson, J. Kirkpatrick, P. Ravirajan, Factors limiting the efficiency of molecular photovoltaic devices, Phys. Rev. B **69** (2004) 035337.
46. F. J. Zhang, A. Vollmer, J. Zhang, Z. Xu, J. P. Rabe, N. Koch, Org. Electron. **8**, 606 (2007).
47. J. C. Blakesley, N. C. Greenham, J. Appl. Phys. **106**, 034507 (2009).
48. J. Hwang, A. Wan, A. Kahn, Mater. Sci. Engineering R, **64**, 1 (2009).

49. H. Frohne, S. E. Shaheen, C. J. Brabec, D. C. Muller, N. S. Sariciftci, K. Meerholz, Chem. Phys. Phys. Chem. **3**, 795 (2002).

50. D. Ofer, R. M. Crooks, M. S. Wrighton, J. Am. Chem. Soc. **112**, 7869 (1990).

51. B. Delgertsetseg, N. Javkhlantugs, E. Erdenebileg, Y. Yokokura, T. Ooba, K. Ueda, C. Ganzorig, and M. Sakomura, Organic Electronics. **23**, 164 (2015).

Figures and Tables

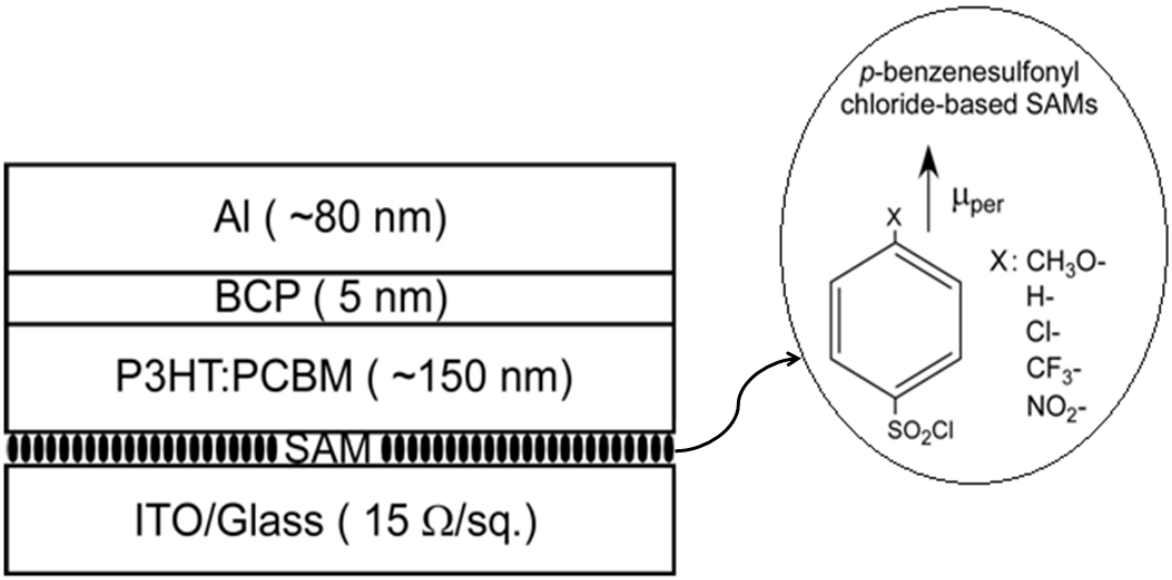

Figure 3.1 A typical device configuration of polymer blend solar cells with SAM-modified structures containing *p*-benzenesulfonyl chlorides with CH_3O-, H-, Cl-, CF_3, and NO_2-groups on ITO electrode surfaces.

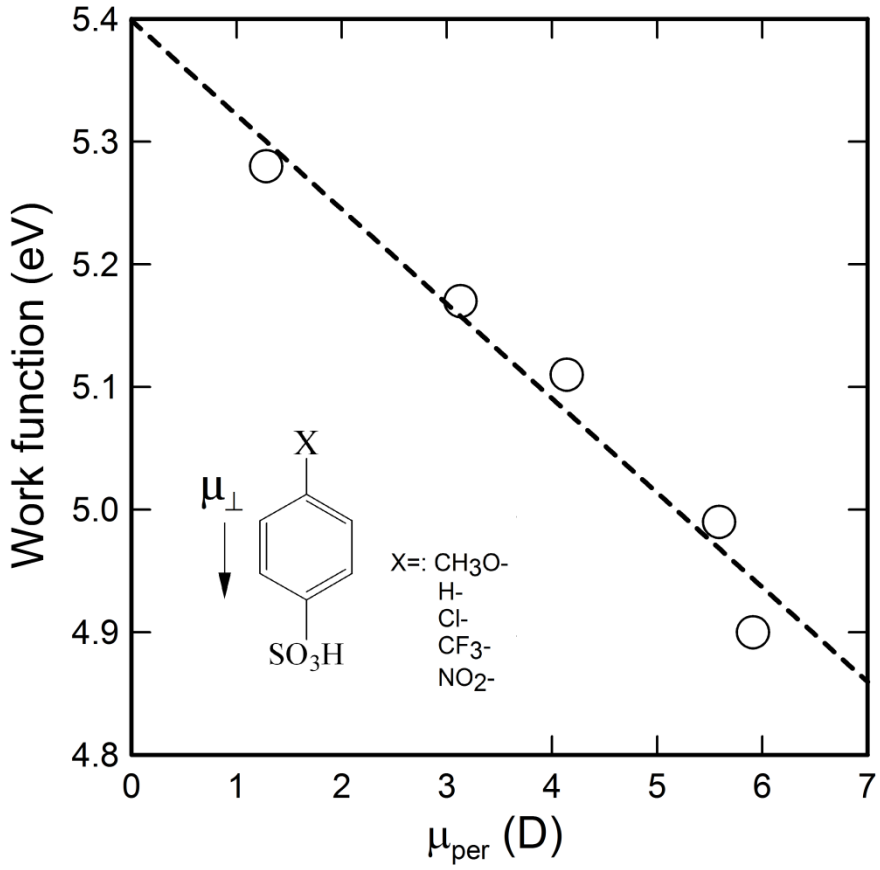

Figure 3.2 Correlation between WF based on measured CPD values and calculated dipole moments for various SAM models.

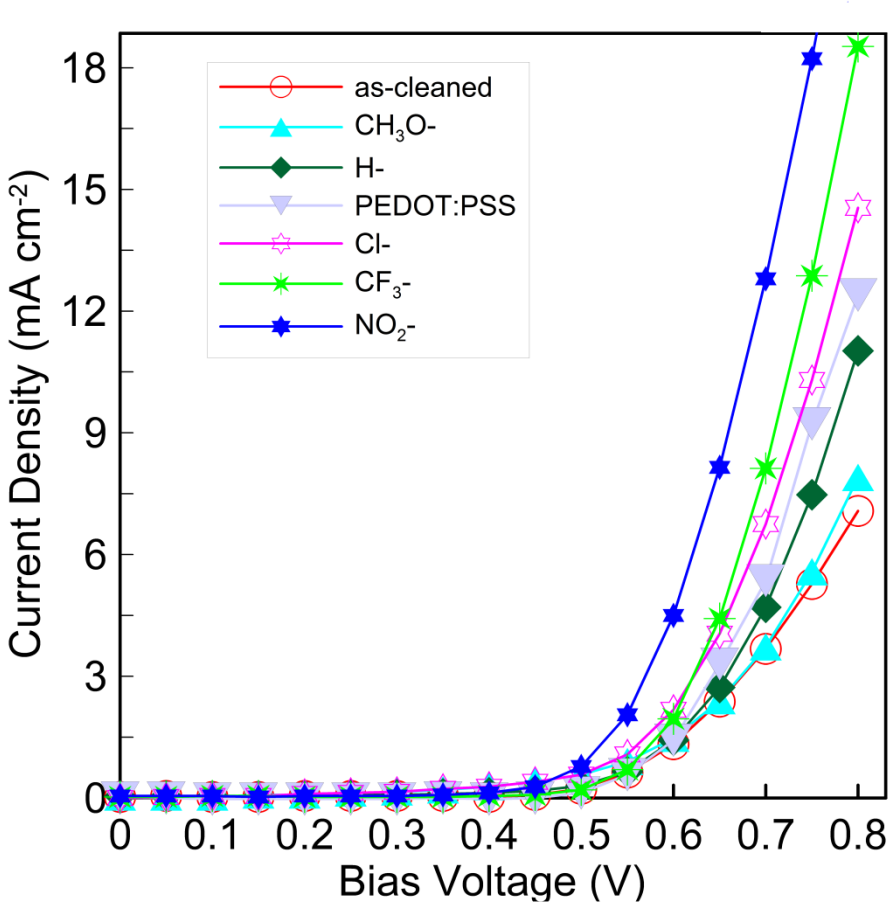

Figure 3.3 Dark current density–bias voltage (J–V_{bias}) characteristics of BHJ PV cells with variously modified ITOs.

(a)

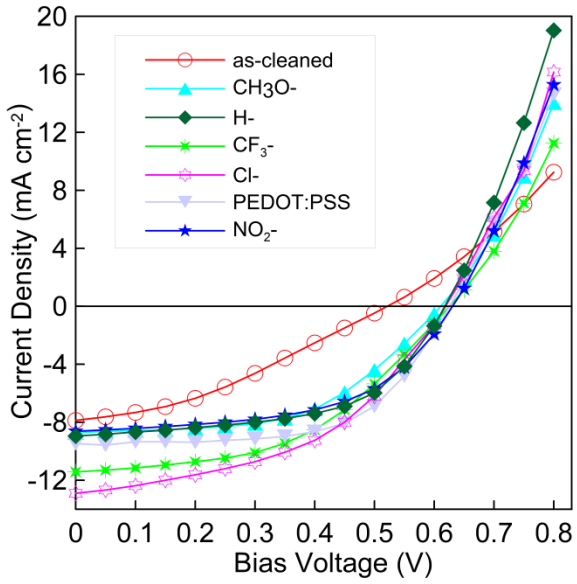

(b)

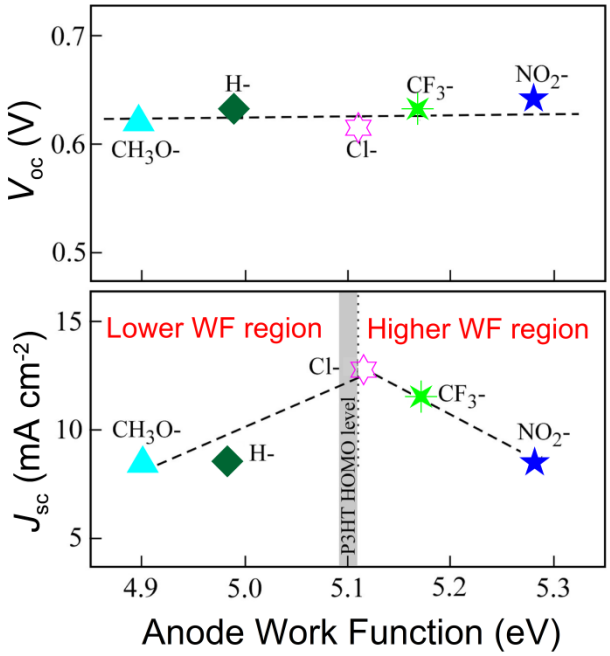

Figure 3.4. (a) J–V_{bias} characteristics of BHJ PV cells with various surface modifications of ITO under simulated AM 1.5 illumination (100 mW cm^{-2}). (b) Plots of measured V_{oc} (upper part) and J_{sc} (lower part) versus anode ITO WF of lower (CH_3O, H, and Cl) and higher (Cl, CF_3, and NO_2) WF regions. The dashed lines serve as guides to the eye.

Table 3.1 Surface potential properties of SAM-modified ITOs and calculated dipole moments for the corresponding SAM molecules.

SAM molecules (**X-C_6H_4-SO_2Cl**)	**ΔV_{CPD}** (**V**)	**Work Function** (**eV**)	**μ_{per}** (**Debye**)
CH_3O-	0.42	4.90	5.91
H-	0.51	4.99	5.59
Cl-	0.64	5.11	4.14
CF_3-	0.69	5.17	3.13
NO_2-	0.81	5.28	1.28

Table 3. 2 Characteristics of BHJ PV cells with structure of ITO (modified with SAM)/P3HT:$PC_{61}BM$(~150 nm)/BCP(5 nm)/Al under illumination.

Modified ITOs	J_{sc} **(mA cm^{-2})**	V_{oc} **(V)**	***FF***	η_P **(%)**
ITO (as-cleaned)	7.88	0.53	0.33	1.40
ITO (CH_3O-)	8.71	0.62	0.52	2.80
ITO (H-)	8.94	0.63	0.50	2.84
ITO (Cl-)	12.82	0.62	0.47	3.72
ITO (CF_3-)	11.62	0.63	0.47	3.39
ITO (PEDOT:PSS)	9.43	0.63	0.61	3.62
ITO (NO_2-)	8.62	0.64	0.54	2.98

Chapter 4

Improvement of Open-Circuit Voltage in Organic Photovoltaic Cells with Chemically Modified Indium-Tin-Oxide Electrode

4.1. Introduction

Organic photovoltaic (PV) cells have been attracted much attention in recent decades due to their potentials as fabrication, low-cost production, and technological advantages of semiconductor materials [1-5]. Since the first report of donor-acceptor heterojunction with a power conversion efficiency (η_p) of about 1 % by Tang [6], new materials and device structures have been developed [7-15] in PV cells. After the first report of organic PV cells, the performances of this type of cells have been significantly improved to reach η_p is in a range of 3-8 % range [8,9,16,17]. However, such efficiency is not sufficient for practical use, and further improvement is required.

In order to enhance PV performance of cell, large open-circuit voltage (V_{oc}) should be obtained. Taima *et al*. [18] introduced a *p*-type semiconductor 5,6,11,12-tetraphenylnaphthacene (rubrene) as en electron donor, which has the highest occupied molecular orbital (HOMO) level of 5.4 eV. They obtained the V_{oc} of 0.91 V [18]. Forrest *et al*. [19] introduced an excellent *p*-type semiconductor boron subphthalocyanine chloride (SubPc) with a low HOMO level of 5.6 eV.

Indium-tin-oxide (ITO) is the most widely used as a transparent anode electrode in organic PV cells [6] due to its high conductivity, work function (WF), and transparency in the visible spectral range. Thus, various surface treatments of ITO have been attempted to change the WF of ITO in order to improve the properties of ITO substrates and control the charge

injection barrier height reviewed in previous reports [20,21]. Although a number of groups have shown that chemical modification of ITO can be used to optimize the performance of organic light-emitting diodes (OLEDs) [20,21], there have been limited attempts to use chemical modification or chemically self-assembled monolayer (SAM) in organic PV cells [22,23].

In the present chapter, we studied the investigation of increase in V_{oc} by controlling the WFs of the anode and cathode electrodes to enhance the PV performance of organic PV cells. We report in this chapter, the use of chemically modified ITO with H- and Cl- terminated benzenesulfonyl chlorides forming effective monolayers and 4-chlorophenyldichorophospate (-P). We examined the correlation between the change in the WF of ITO and the performance of the organic PV cells by the chemical modification and find that the large increase in V_{oc}. In order to achieve our purpose, we selected tris(8-hydroxyquinoline)aluminum (Alq_3) as an electron transport layer (ETL) to substitute for bathocuproine (BCP) in cells based on rubrene(Rub)/buckminsterfullerene (C_{60}) heterojunction. Moreover, in order to examine the further improvement of V_{oc}, we used a lithium carboxylate (C_6H_5COOLi) [24] as a cathode interface material with low WF was inserted between ETL and Al.

4.2. Experimental

ITO coated glass substrates with a sheet resistance of *ca*. 15 Ω/square (Sanyo Vacuum Industries) were cleaned by sonication successively in two detergents (Extran MA 03, pH 6.8, MERCK and Kontaminon O, pH 10, WAKO), rinsed with deionized water, and stored in isopropanol until being required. After cleaning with acetone and isopropanol (this cleaned ITO will be called hereafter "as-cleaned ITO") the ITO substrates were immersed for 5 min in dichloromethane solutions containing 1 mM of benzenesulfonyl chloride or 4-

chlorobenzenesulfonyl chloride (Tokyo Chemical Industry) and 4-chlorophenyldichorophospate (Tokyo chemical industry). The modified ITO anodes were rinsed in pure dichloromethane and then vacuum dried for ~1 h.

C_{60} (purity>99 %) (Tokyo Chemical Industry), the sublimed grade rubrene (Aldrich Co.) and Alq_3 (Dojindo Labs), the reagent grade BCP (Kanto Chemical), and lithium benzoate (purity~99 %) (Aldrich Co.) were used without further purification. All the materials were deposited using vacuum evaporation under a pressure of $5\text{-}7\times10^{-6}$ Torr at deposition rates of 1-1.5 Å/s for organic layers and 3-4 Å/s for Al cathode. The active area for all the cells was defined to be 5×5 mm^2 by using a shadow mask. The current density-voltage (*J-V*) curves were measured under illumination of a simulated solar light with 100 $mW\times cm^{-2}$ (AM1.5G) by a solar simulator (Yamashita Denso, YSS-50). Electric data were taken using an Advantest R6145 DC voltage current source unit at room temperature in ambient atmosphere.

4.3. Results and Discussion

4.3.1. Expected energy diagrams of PV cells

For a cell based on exciton dissociation by charge transfer at a donor-acceptor (D/A) interface, η_p is the product of the efficiencies [1] of four sequential steps (*i*) photon absorption leading to the generation of an exciton, (*ii*) diffusion of the exciton to the D/A interface, (*iii*) exciton dissociation (or charge separation) by charge-transfer (CT) at the D/A interface, and (*iv*) collection of the free charge carriers at electrodes, i.e., charge transport to the anode (holes) and cathode (electrons), to supply a direct current.

Fig. 4.1 shows the interfacial energy diagrams with shifts of vacuum level (Δ) at the interfaces due to dipole layer formation in four types of cells studied in the present work. In

general, the WF of metal is changed by covering the metal surface with different materials [25]. First, we will discuss the shift at a C_{60}/Al cathode interface. The photoemission study of the C_{60}/Al interface revealed [26] an abrupt vacuum-level shift of $\Delta = \sim +0.9$ eV. Namely, the WF of the Al electrode (4.2 eV) was increased to 5.1 eV by depositing a C_{60} film on an Al surface. This shift is schematically illustrated in **Fig. 4.1 (a)-(b).** The same energy level shift at the C_{60}/Al interface was also reported previously [27]. Another group reported the shift of +0.7 eV for the C_{60}/Al interface and that of +0.9 eV for the C_{60}/LiF(0.5 nm)/Al interface [28]. In the latter case, the WF was increased from 3.6 eV (LiF/Al) to 4.5 eV (C_{60}/LiF/Al). The increase in the WF for all cases described above is possibly interpreted by partial electron transfer from Al to C_{60} [26-28]. The HOMO and the lowest unoccupied molecular orbital (LUMO) level of C_{60} are reported to be 6.2 eV and 3.7 eV, respectively [10]. The increase in the work function of the Al electrode, however, is not preferable to create the built-in potential (V_{bi}) to separate the charge effectively in the organic PV cells.

In order to decrease the WF of the Al electrode, we have to put another layer of less electron affinity than C_{60}. As such materials, we examined Alq_3 and BCP [10,16,20,29-31] LUMO levels of which are higher (i.e., less electron affinity) than that of C_{60}. In fact, the organic side for these interfaces is charged positively, making this side more comfortable (low energy) for an electron, and making the sign of Δ negative. Taking into account the Δ at Alq_3/Al interface of ~ -1.0 eV [25], the resulting WF of Alq_3/Al is decreased from the value of metallic Al (4.2 eV) [16] down to 3.2 eV as shown in **Fig. 4.1(c)-(d).** The WF of the LiF/Al substrate was also gradually decreased upon Alq_3 deposition, from 3.6 eV to 3.1 eV for Alq_3 film deposition [28,32]. Toyoshima *et al.* reported the electronic structure at the interface between BCP and Al by UV photoemission spectroscopy **[**33]. Their results for

BCP/Al interface were similar to the shift in the WF as observed at Alq_3/Al interface [25,32]. In this way, we constructed the energy diagrams of the Al cathode side as shown in **Fig.4.1.**

Next, we discuss the WF control of the anode side. The molecular approach allows for fine-tuning the WF using organic molecules on ITO depending upon magnitude and direction of the dipole moment [34]. The effective WFS formed by chemical modification of ITO shown in **Fig. 4.1** were estimated from the contact potential difference (CPD) values [34,35].

An interface dipole with its negative end pointing toward the organic layer and its positive end toward the electrode surface increases the ITO work function (i.e., the Fermi energy is down) and HOMO energy level in the organic layer is relatively up by adding an electrostatic energy [8] as shown in **Fig. 4.1.** When the cells studied have the same cathode material, the changes in V_{bi} obtained for cells with variously modified ITO electrodes are equal to the changes in the ITO WF. This is illustrated on the left side of **Fig. 4.1**, where we consider that the ITO work function is in the range 4.5-5.0 eV The HOMO and LUMO values for rubrene are reported to be 5.4 eV and 3.2 eV, respectively [18]. The WF control at the anode as well the cathode leads to buildup of a large V_{bi} as shown in **Fig. 4.1(d).** The dipole layers at interfaces may have a deep impact on the V_{bi} and consequently on the V_{oc} of organic PV cells.

4.3.2. Characteristics of PV cells

Fig. 4.2 shows the effect of ITO WF on the J-V_{bias} characteristics under 100 mw cm^{-2} illumination and in dark of four kinds of the PV cells with various surface treatments of ITO. **Fig. 4.2(a)** shows the room temperature J-V_{bias} characteristics of ITO(variously treated)/C_{60}(60 nm)/Al single-layer cells with a focus on the dark conduction properties. A linear fitting of the log-log plot (not shown) for these cells shows that the current for forward bias (electrons injection from the top contact) increases much slower (a slope is ~1) than the

space-charge limited conduction (SCLC) [36]. Conducting charge transfer complex formed on C_{60}/metal interface was studied in Ref.[37]. The gap state, pinning the Fermi level close to the LUMO of C_{60} molecule, is originating from the C_{60}-metal complex formation at the interface [37]. The unoccupied states of the C_{60}-metal complex appeared between the Fermi level and LUMO of C_{60} molecules lower the injection barrier which directly explains the improved device characteristics [37].These states lead to the formation of Ohmic contact at the C_{60}/Al. A thin LiF interlayer inserted between C_{60} film and Al cathode gave an effective passivation for the contacts by preventing Al oxidation [38]. It appears that a thin interlayer can help to perverse the SCLC in C_{60} film and cells under exposure to air, by considerably suppressing the oxygen diffusion into the C_{60} film and reaction at the C_{60}/Al interface [38].

In **Fig. 4.2(b)-(c),** the V_{oc} was most effectively increased when Cl-terminated benzenesulfonyl chloride was used. With ITO modified with H-terminated benzenesulfonyl chloride without any appreciable dipole moment in the *para*-position, the characteristics of the organic PV cells were much better than those on as-cleaned ITO. From the results, the PV characteristics, in particular the V_{oc}, which were well correlated with the WF change, were dramatically improved by the chemical modification of ITO.

The changes in V_{oc} resulting from changes in the self-assembling dipole molecules used to coat the ITO surfaces follow the WF changes for the resulting ITO electrodes; higher WF anodes result in larger values of the V_{oc} in the cells studied in the present work. In **Fig. 4.2(c)**, it can be seen, for example, that the V_{oc} can be increased from 0.35 V (as-cleaned ITO) to 0.48 V by grafting benzenesulfonyl chloride onto the ITO electrode. By grafting a monolayer of Cl-terminated benzenesulfonyl chloride molecules results in a further increase in the V_{oc} to 0.84 V.

A dramatic effect of Alq_3(10 nm) or BCP(10 nm) as a buffer layer deposited between C_{60} and Al on the measured J-V_{bias} characteristics is clearly observed in **Fig. 4.2(b)-(d).** The PV cells with Alq_3 or BCP exhibited the best J-V_{bias} characteristics and gave the typical diode characteristics. BCP is the material selected as an exciton blocking layer [16]. Alq_3 is a good ETL material widely used in OLEDs [34]. It can be seen in **Fig. 4.2(c)-(d)** that the cells exhibited similar PV characteristics, indicating that band gaps and LUMO levels of the materials of Alq_3 and BCP have minor effects on the PV performances. As shown in **Fig. 4.1c,** while bandgaps and LUMO levels of Alq_3 and BCP are different, the performance of the cells is not significantly changed by different ETL materials (**Table 4.1**). This indicates that electron transport in these cells should not be via LUMO levels of these ETL materials. The results suggest that the most important role of Alq_3 or BCP is to establish an ohmic contact between Al and C_{60} i.e., a protective film on C_{60} [39].

While alkali metal-doped organic materials such as Alq_3 have been used as an ETL in OLEDs [40,41] this approach has not been explored in organic PV cells. Recently, we observed the alkali metal formation by thermal decomposition during vapor deposition of alkali metal carboxylates without post-deposition of Al cathode [42]. The improvement was attributed to the reaction of hot Al atoms with C_6H_5COOLi to form metallic Li during Al vapor deposition [41]. The resulting metallic Li was believed to dope the Alq_3 layer [40] and to alloy with the Al cathode [24]. To examine the influence of induced V_{bi} on the performance of the cells, a 2 nm C_6H_5COOLi as a cathode interface material deposited between C_{60} or C_{60}/Alq_3 (or C_{60}/BCP) and Al cathode was used. The J-V_{bias} characteristics of the ITO(modified with Cl-)/Rub(20 nm)/C_{60}(40 nm)/Al with variously configured cathodes under 100 mW cm^{-2} illumination is shown in **Fig. 4.3.** The PV performances of the cells are summarized in **Table 4.1.** Among all the cells studied, we found that the large increase in V_{oc}

for the ITO(modified with Cl-)/Rub(20 nm)/C_{60}(40 nm)/Alq_3(10 nm)/Li/Al cell. We obtained the V_{oc} of 0.92±0.1 V.

In **Fig. 4.3** and **Table 4.1**, the V_{oc} of cell with the Alq_3/Li/Al is the highest, and followed by the BCP/Li/Al, Alq_3/Al or BCP/Al, Al, and C_6H_5COOLi/Al cells. The results suggest the importance of lower WF of Li (2.9 eV) [41] for the larger V_{oc}. The V_{bi} is increased to larger value, giving an interfacial dipole, which may be attributed to both the alloy formation at the Al cathode [24,41] and doping of Alq_3 with Li [40-43]. The ITO(modified with Cl-)/Rub(20 nm)/C_{60}(40 nm)/Li/Al cell exhibited the lowest V_{oc}. It may be considered, however, from our recent study of quenching by the presence of excess and colored species[44] that the doping of C_{60} with Li increases exciton quenching and so that more excitons cannot contribute to the generation of electricity. Srdanov et al [45] reported results of an in-situ optical absorption study on alkali metal-doped thin films of C_{60}.

Gregg and Hanna [46] proposed that the V_{oc} is controlled by a chemical potential energy gradient of the organic PV cells. The chemical potential gradient is equivalent to the carrier concentration gradient and would depend on the carrier mobility. Based on this idea, V_{oc} is dependent on the hole mobility [47] The built-in electrical potential still plays a role in most organic PV cells. Both the chemical potential and the electrical potential must be taken into account [46].

In two-layer organic PV cells, the V_{oc} scales linearly with the work function difference, however, with an additional contribution depending on the light intensity. This contribution is due to the accumulation of charge carriers at the D/A interface, giving rise to a diffusion current which must be compensated by a drift current at open circuit [48]. Under illumination, charges are separated across the D/A interface. Due to the concentration gradient, carriers will

diffuse away from the interface, leading to a net diffusion current. The effect of diffusion on V_{oc} in single-layer PV cells has been studied by Malliaras et al [49]. The accumulated charges at the interface will create a band-bending, which leads to a reduction of the electric field in the bulk of the cell.

In addition to attempts to optimize the components and composition of the active layer, modification of the electrodes has also lead to an improvement in device performance [50]. It is evident that the WF of the negatively charged electrode is relevant for the V_{oc} of the cells. In the classical metal-insulator-metal (MIM) concept, the V_{oc} is in first order approximation governed by the WF difference of the anode and the cathode, respectively. It should be noted that this only holds for the case where the Fermi levels of the contacts are within the bandgap of the insulator and are sufficiently far away from the HOMO and the LUMO levels, respectively [51]. In the case of ohmic contacts, meaning that the negative and positive electrodes match the LUMO level of the acceptor and the HOMO level of the donor, respectively, the situation is different; charge transfer of electrons or holes from the metal into the semiconductor occurs in order to align the Fermi level at the negative and positive electrode, respectively [51]. As a result, the electrode WFs becomes pinned close to the LUMO/HOMO level of semiconductor [50]. Because of this pinning, the V_{oc} will be governed by the energetics of the LUMO of the acceptor and the HOMO of the donor. Indeed, in bilayer cells, a linear correlation of the V_{oc} with the reduction potential of the acceptor has been reported [52].

For cells with non-ohmic contacts, the observed V_{oc} is in agreement the expected values [50]. In this case, the V_{oc} is determined by the work function differences of the electrodes. However, for the ohmic contact the measured value is lower that the predicted value, possibly due to the energetic disorder of the charge transport levels [50]. Furthermore, generation of

free charges is enhanced by an electric field in the appropriate direction. Possible mechanism by which balance between electron and hole escape currents can be maintained in the steady state is by the build-up of a net charge density within the cell. This acts to reduce the electric field (and hence suppress the generation of free charges) at one electrode and increase it at the other [53]. Snaith et al. [53] found that a charge injection barrier from electrodes into the polymer film helps to retain a high V_{oc} in the blend cell.

Conclusion

We have studied the use of chemically modified ITO with 4-chlorophenyldichorophospate (-P) and H- and Cl-terminated benzenesulfonyl chlorides forming effective monolayers to control the WF of ITO for enhancing the V_{oc} in organic PV cells. We have examined the correlation between the change in the WFs of electrodes and the performance of the organic PV cells before and after the surface modification and found that the large increase in V_{oc} for the ITO(modified with Cl-)/Rub(20 nm)/C_{60}(40 nm)/Alq_3(10 nm)/C_6H_5COOLi(2 nm)/Al. We obtained the V_{oc} of 0.92±0.1 V. Controlling the WFs of electrodes by surface modification at the interfaces is a key parameter, which is useful for interpreting the origin of V_{oc} and leads to improvements in the J-V_{bias} characteristics of the organic PV cells.

References

1. P. Peumans, A. Yakimow and S. R. Forrest, J. Appl. Phys. **93**, 3693 (2003).
2. S. R. Forrest, Nature. **428**, 911 (2004).
3. T. Kietzke, Advances in Optoelectronics. Vol. 2007, 1 (2007).
4. J. Xue, Polym. Rev. **50**, 411 (2010).
5. F. C. Krebs, "Polymeric Solar Cells: Materials, Design, Manufacture", DEStech Publications, Inc., Lancaster, PA, 2010.
6. C. W. Tang, Appl. Phys. Lett. **48**, 183 (1986).
7. Z. R. Dai, Z. W. Pan and Z. L. Wang, Adv. Funct. Mater. **13**, 9 (2003).
8. J. Xue, S. Uchida, B. P. Rand and S. R. Forrest, Appl. Phys. Lett. **84**, 3013 (2004).
9. J. Xue, S. Uchida, B. P. Rand and S. R. Forrest, Appl. Phys. Lett. **85**, 5757 (2004).
10. K. L. Mutolo, E. I. Mayo, B. P. Rand, S. R. Forrest and M. E. Thompson, J. Am. Chem. Soc. **128**, 8108 (2006).
11. G. Dennler, M. C. Scharber and C. J. Brabec, Adv. Mater. **21**, 1323 (2009).
12. H. Y. Chen *et al.,* Nat. Photon. **3**, 649 (2009).
13. G. E. Morse and T. P. Bender, ACS Appl. Mater. Interfaces. **4**, 5055 (2012).
14. G. Li, R. Zhu and Y. Yang, Nat. Photon. **6**, 153 (2012).
15. J. Yang, L. Qian, R. Zhou, Y. Zheng, A. Tang and P. H. Holloway, J. Appl. Phys. **111**, 044323 (2012).
16. P. Peumans and S. R. Forrest, Appl. Phys. Lett. **79**, 044323 (2001).
17. M. A. Green, Keith Emery, Yoshihiro Hishikawa, and W. Warta "Solar cell efficiency tables (version 37)", Prog. Photovol. **19**, 84 (2011).
18. T. Taima, J. Sakai, T. Yamanari, and K. Saito, Jpn. J. Appl. Phys. **45**, L995 (2006).

19. K. L. Mutolo, E. I. Mayo, B. P. Rand, S. R. Forrest, and M. E. Thompson, J. Am. Chem. Soc. **128**, 8108 (2006).
20. M. Fujihira and C. Ganzorig, in Conjugated Polymer and Molecular Interfaces, edited by A. Kahn, J. J. Pireaux, W. R. Salaneck, and K. Seki, (Marcel Dekker, New York, 2002), p. 817-858.
21. C. Ganzorig and M. Fujihira, in "Chemically Modified Oxide Electrodes", "Modified Electrodes" edited by A. J. Bard and M. Stratmann, Encyclopedia of Electrochemistry, Vol. **10**, WILEY-VCH Verlag GmbH, Weinheim (2007), pp. 261-334.
22. N. R. Armstrong *et al.,* Thin Solid Films. **445**, 342 (2003).
23. S. Khodabakhsh, B. M. Sanderson, J. Nelson and T. S. Jones, Adv. Funct. Mater. **16**, 95 (2006).
24. C. Ganzorig and M. Fujihira, Jpn. J. Appl. Phys. **38**, No. 11B, L1348 (1999).
25. H. Ishii, K. Sugiyama, E. Ito and K. Seki, Adv. Mater. **11**, 605 (1999).
26. A. J. Maxwell, P. A. Bronwiler, D. Arvanitis, J. Hasselstrom, M. K. J. Johansson and N. Martensson, Phys. Rev. B. **57**, 7312 (1998).
27. J. Y. Lee, Appl. Phys. Lett. **88**, 073512 (2006).
28. S. K. M. Jonsson, W. R. Salaneck and M. Fahlman, J. Appl. Phys. **98**, 014901 (2005).
29. R. Mitsumoto *et al.,* J. Phys. Chem. A. **102**, 552 (1998).
30. M. Hayashi, H. Ishii, Y. Ouchi, and K. Seki, J. Appl. Phys. **92**, 3784 (2002).
31. Y. Tanaka, K. Kanai, Y. Ouchi, and K. Seki, Chem. Phys. Lett. **441**, 63 (2007).
32. T. Yokoyama, D. Yoshimura, E. Ito, H. Ishii, Y. Ouchi and K. Seki, Jpn. J. Appl. Phys. **42**, 3666 (2003).
33. S. Toyoshima, K. Kuwabara, T. Sakurai, T. Taima, K. Saito, H. Kato, and K. Akimoto, Jpn. J. Appl. Phys. **46**, 2692 (2007).

34. C. Ganzorig, K. J. Kwak, K. Yagi, and M. Fujihira, Appl. Phys. Lett. **79**, 272 (2001).

35. Kh. Sarangerel, C. Ganzorig, M. Fujihira, M. Sakomura, and K. Ueda, Chem. Lett. **37**, 778 (2007).

36. C. Ganzorig, M. Sakomura, K. Ueda, and M. Fujihira, Appl. Phys. Lett. **89**, 263501 (2006).

37. S. W. Cho et al*.,* Synth. Met. **157**, 160 (2007).

38. C. J. Huang, D. Glozea, A. Turakn and Z. H. Lu, Appl. Phys. Lett. **86**, 033107 (2005).

39. M. Vogel, S. Doka, Ch. Breyer, M. Ch. Lux-Steiner, and K. Fostiropoulos, Appl. Phys. Lett. **89**, 163501 (2006).

40. J. Kido and T. Matsumoto, Appl. Phys. Lett. **73**, 2866 (1998).

41. C. Ganzorig, K. Suga, and M. Fujihira, Mater. Sci. Eng. B, **85**, 140 (2001).

42. C. Ganzorig and M. Fujihira, Appl. Phys. Lett. **85**, 4774 (2004).

43. N. Johansson, T. Osada, S. Stafstrom, W. R. Salaneck, V. Parente, D. A. dos Santos, X. Crispin, and J. L. Bredas, J. Chem. Phys. **111**, 2157 (1999).

44. C. Ganzorig and M. Fujihira, Appl. Phys. Lett. **81**, 3137 (2002).

45. V. I. Srdanov, C. H. Lee, and N. S. Sariciftci, Thin Solid Films. **257**, 233 (1995).

46. B. A. Gregg and M. C. Hanna, J. Appl. Phys. **93**, 3605 (2003).

47. Y. Terao, H. Sasabe and C. Adachi, Appl. Phys. Lett. **90**, 103515 (2007).

48. C. M. Ramsdale *et al.,* J. Appl. Phys. **92**, 4266 (2002).

49. G. G, Malliaras, J. R. Salem, P. J. Brock, and J. C. Scott, J. Appl. Phys. **84**, 1583 (1998).

50. V. D. Mihailetchi, P. W. M. Blom, J. C. Hummelen, and M. T. Rispens, J. Appl. Phys. **94**, 6849 (2003).

51. P. W. M. Blom, V. D. Mihailetchi, L. J. A. Koster, and D. E. Markov, Adv. Mater. **19**, 1551 (2007).

52. C. J. Brabec *et al.,* **11**, 374 (2001).

53. H. J. Snaith, N. C. Greenham, and R. H. Friend, Adv. Mater. **16**, 1640 (2004).

Figures and Tables

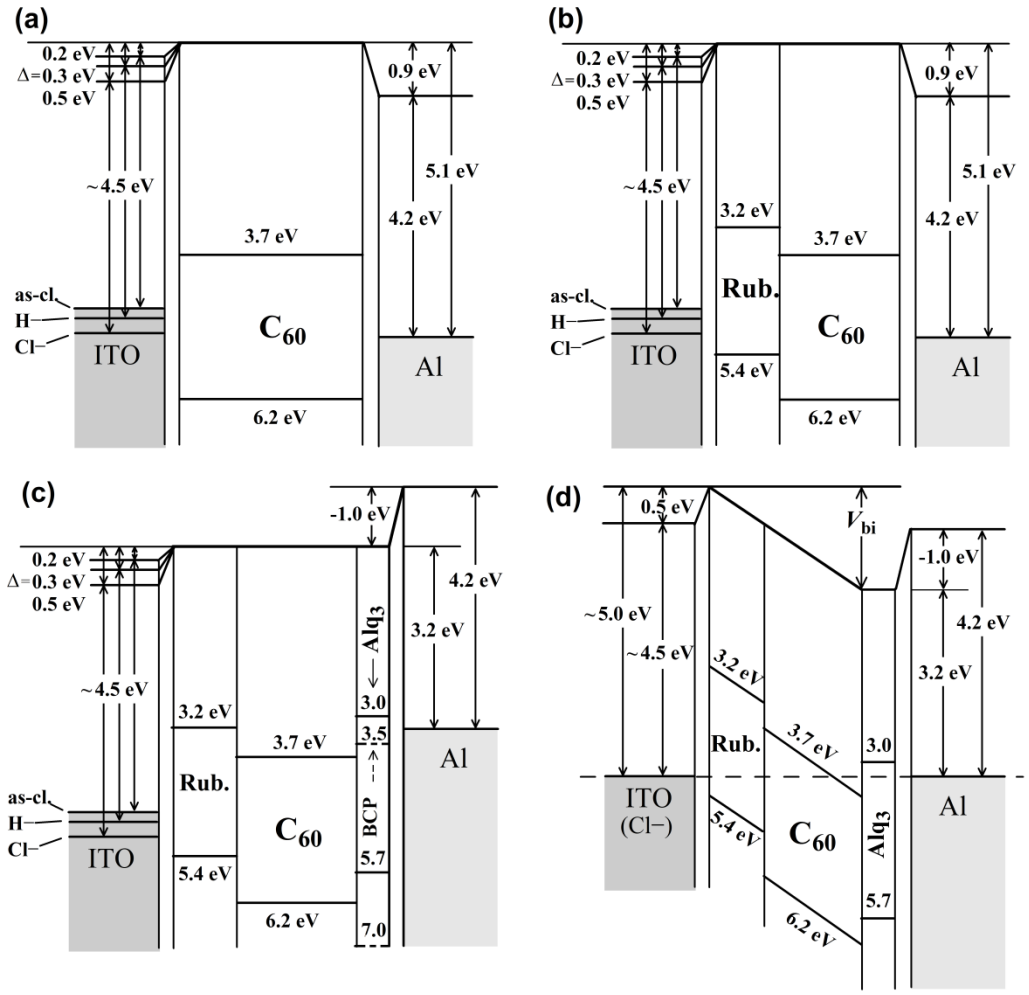

Fig. 4.1 Interfacial energy diagrams with the shifts of vacuum level (Δ) at the interfaces due to dipole layer formation in the organic PV cells. The effective WFs of chemically modified ITO were estimated from the CPD values. At the C_{60}/Al interface, the WF of Al is changed by covering the metal surface with different organic materials. The organic side is charged positively, making this side more comfortable (low energy) for an electron, and making the sign of Δ negative. These lead to buildup of built-in potential (V_{bi}) as shown in (d).

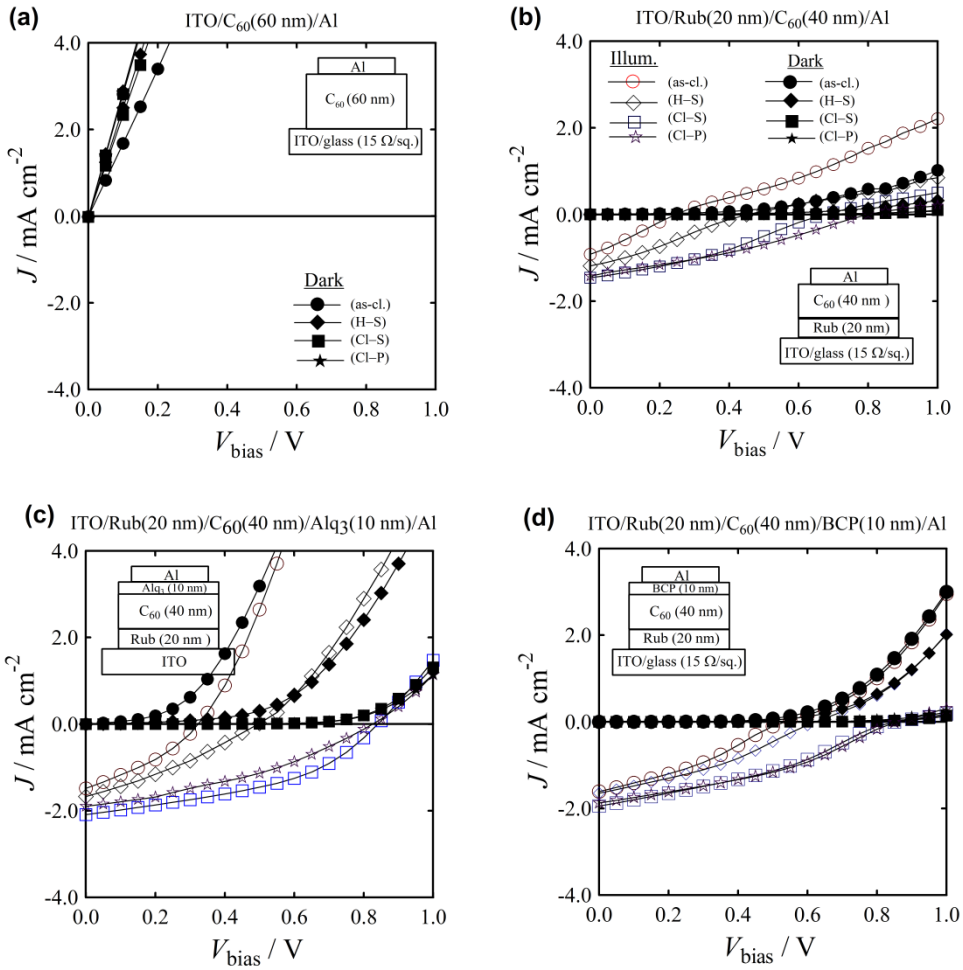

Fig. 4.2. The effect of ITO work function on the J-V_{bias} characteristics under AM 1.5 illumination (100 mW cm^{-2}) and in dark of the cells with various surface treatments of ITO: a) single-layer C_{60}, b) two-layer Rub/C_{60}, and three-layers (c) with Alq_3, and (d) with BCP.

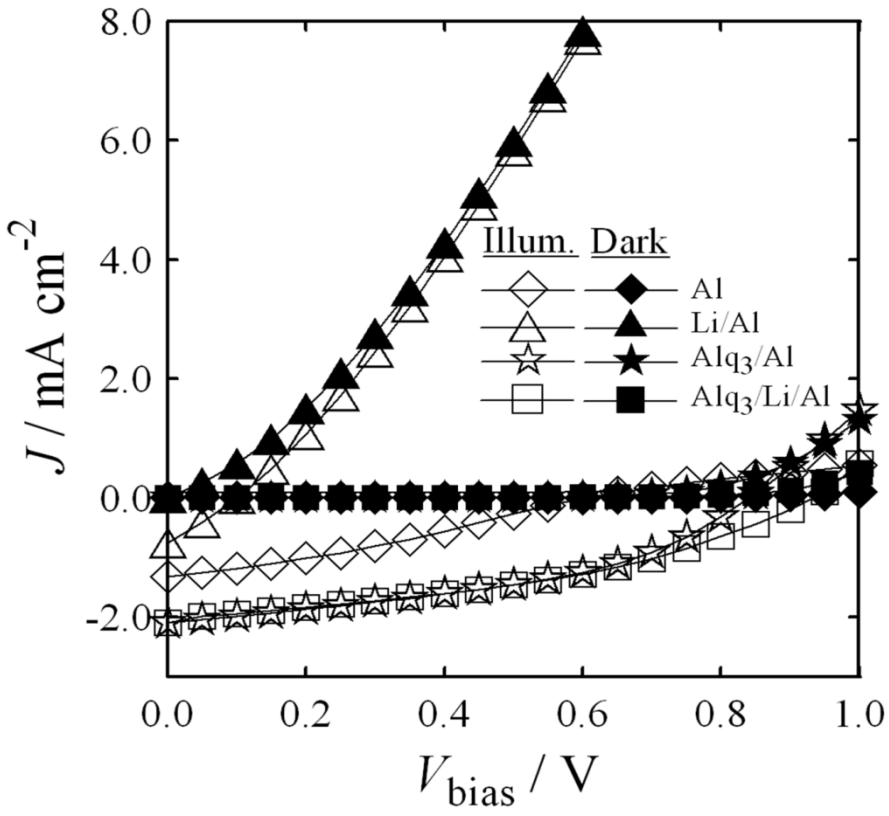

Fig. 4.3 J-V_{bias} characteristics of the ITO(modified with Cl-)/Rub(20 nm)/C_{60}(40 nm)/Al with variously configured cathodes under AM 1.5 illumination (100 mW cm^{-2}) and in dark.

Table 4.1 The performances of organic PV cells with a structure of ITO(modified with Cl-)/Rub(20 nm)/C_{60}(40 nm)/Al with different configured cathodes under 100 mW cm^{-2} illumination.

Cathode structures	J_{sc} **(mAcm^{-2})**	V_{oc} **(V)**	**FF**	η_p **(%)**
Al	1.46	0.68	0.37	0.36
C_6H_5COOLi(2 nm)/Al	0.80	0.21	0.37	0.06
BCP(10 nm)/Al	1.95	0.85	0.35	0.58
BCP(10 nm)/C_6H_5COOLi(2 nm)/Al	2.06	0.82	0.43	0.73
Alq_3(10 nm)/Al	2.09	0.84	0.45	0.79
Alq_3(10 nm)/C_6H_5COOLi(2 nm)/Al	2.10	0.93	0.40	0.78

Chapter 5

Effect of Bathocuproine Electron-Transport Layer in Organic Photovoltaic Cells with Laminated Top Electrode

5.1 Introduction

Organic photovoltaic (PV) cells have attracted increasing attention as promising devices because of their mechanical flexibility, ease of fabrication, and potential for inexpensive production. Since the donor-acceptor concept of inorganic p-n junctions has been successfully adopted into organic PV cells by Tang [1] and Yu *et al.,* [2] the power conversion efficiency of thin-film organic PV cells has increased steadily and rapidly.

To enhance the power conversion efficiencies of small-molecule organic PV cells composed of bilayer structures of donor and acceptor organic semiconductors formed by vapor deposition processes, bathocuproine (BCP) has been known as one of the most effective electron-transport layer (ETL) materials inserted between the acceptor layer and a metal electrode. **Fig. 5.1** illustrates a structure of organic PV cells with BCP layer (a) and the corresponding energy diagram (b). In this structure zinc phthalocyanine (ZnPc) and fullerene (C_{60}) are used as a *p*-type donor and a *n*-type acceptor material, respectively. The insertion of 5-10 nm BCP layer is known to enhance the electron transport to the metal cathode from the adjoining acceptor layer while effectively blocking excitons in the acceptor layer from recombining at the cathode [3].

Peumans and Forrest [4] suggest that during vacuum deposition of metallic cathode defect states below the lowest unoccupied molecular orbital (LUMO) of BCP (3.5 eV) would be induced into the BCP layer. If the electron transport is via the LUMO level of BCP (i.e., path i

illustrated in **Fig. 5.1(b**) the electrons at the LUMO level of C_{60} (4.5 eV) must overcome the energy barrier of 1.0 eV to reach cathode. On the other hand, the defect states can provide a lower energy path for electrons toward the cathode (path ii in **Fig. 5.1b**). To explain the effective electron transport without incurring a substantial voltage decreases, the formation of metal induced defect states in ETLs has been proposed to be responsible for the electron transport in the BCP layer; however, the exact mechanisms of ETL functions are still not clear

Oida and Harafuji recently investigated the electron-transport mechanism through the BCP layer by using inverted structure devices of ITO/thin cathode metal (Ag or Au)/BCP/ C_{60}/copper phthalocyanine (CuPc)/pentacene/anode metal (Ag) [5]. The pentacene layer inserted between the CuPc donor layer and top metal layer acts as a buffer layer that modifies the work function (WF) of the top electrode so that the top electrode plays the role of an anode [6]. They observed that the series resistance in the inverted device was as low as that in a device with the normal structure, anode ITO/pentacene/CuPc/C_{60}/BCP/cathode metal (Ag).

Wang *et al.,* investigated the electronic properties of Ag/BCP (0.8 nm)/C_{60} (0-5 nm) heterostructures prepared by successive depositions of BCP and C_{60} on Ag by synchrotron-based in situ ultraviolet photoemission spectroscopy (UPS) [7]. Their results indicated the presence of gap states in the region of nearby the BCP-C_{60} interface originated from Ag-BCP complex formed when BCP was deposited on Ag. Therefore, the gap states in BCP would be present to some extent even in the inverted organic PV cells produced by vacuum vapor depositions of the organic layers and the metal layers.

In the present chapter, we report that the normal structure device of anode ITO/ ZnPc/C_{60}/BCP/cathode metal (Au) formed with a laminated top electrode to suppress the cathode-induced defect states in the BCP layer.

5.2. Experimental

Fig. 5.2 schematically illustrates the fabrication procedures of our laminate organic PV cells. The elastomeric substrate of the top cathode component was obtained by curing poly(dimethylsiloxane) (PDMS) (Dow Corning, Silpot 184) on a Si wafer. Onto the smooth surface of the PDMS substrate removed from the Si wafer, a 100-nm-thick Au layer was deposited through a shadow mask by vacuum evaporation. Bowden *et al*., reported the spontaneous formation of a wave surface of a Au film deposited on a PDMS substrate by electron beam evaporation [8]. They suspected that thermal contraction of the PDMS substrate would cause the Au film to buckle on cooling. This buckling can be prevented by mounting the PDMS substrate at a distance from the metal source that is sufficient to limit thermal heating [9].

In our resistive thermal evaporator, the distance of 18 cm was sufficient to obtain a flat Au coating on the PDMS substrate. The bottom anode components with and without BCP layer were prepared by sequential vapor deposition of a 30 nm ZnPc layer, a 40 nm C_{60} layer, and a 0 or 10 nm BCP layer on ITO substrate without breaking the vacuum. The anode and the cathode components were successively prepared in the same vacuum bell jar.

The film thicknesses were monitored by using a quartz oscillator located next to the ITO and the PDMS substrates. Finally, the formation of the top cathode over the C_{60} or the BCP layer of the bottom component was carried out in an ambient atmosphere by the physical contact of the PDMS substrate with metal stripe of Au. To establish the contact, neither external pressure nor heat was required. In order to minimize contamination of the deposited gold and organic films by ambient air, the final process of contacting the cathode and the anode components was carried out within 1 min after taking them out from the vacuum bell jar, which is thoroughly purged beforehand with gaseous nitrogen.

A conventional device with a top electrode formed by successive vacuum evaporation of Au directly onto a BCP layer was also fabricated to compare its PV performance with that of the lamination-type device. The organic layers and the top electrode of the reference evaporation-type device with the structure consisting of ITO/ZnPc/C_{60}/BCP/Au have the same thickness as those of the corresponding lamination-type device.

5.3. Results and Discussion

In **Fig. 5.3(a),** the current density-voltage (*J-V*) characteristics of the lamination- and evaporation type devices with the layer structure ITO/ZnPc (30 nm)/C_{60} (40 nm)/Au (100 nm) are compared under 1 sun AM 1.5 G simulated solar illumination condition (Yamashita Denso YSS-50A). The *J-V* curve of the evaporation-type device without BCP exhibits an almost linear increase, which is presumably due to the reduction in the shunt resistivity induced by the diffusion of cathode metal into the C_{60} layer during the vapor deposition process [10]. Significantly deteriorated PV performances, short-circuit current density (J_{sc}) = 1.65 mA cm^{-2}, open-circuit voltage (V_{oc}) = 0.064 V, fill factor (FF) = 0.255, and power-conversion efficiency (η_p) = 0.027 % were observed with the evaporation-type device without BCP layer. On the other hand, the lamination-type device without BCP layer exhibits improved PV performance with J_{sc} of 3.20 mA cm^{-2}, V_{oc} of 0.374 V, FF of 0.235, and η_p of 0.280%. This result reveals that the formation of the laminated top electrode is profitable to avoid the damage to the organic layer of C_{60} caused by the deposition of thermally evaporated metal cathode layer.

The *J-V* curve of the lamination-type device in **Fig. 5.3(a)** follows an “s shape” with low FF. This kind of *J-V* behavior can be commonly observed with the devices consisting of multilayer structures, including direct contact between C_{60} layer and metal cathode [4,11,12].

The C_{60}-cathode contacts possibly induce the formation of charge transfer states or covalent bonds between C_{60} and metal cathodes; then, the extraction of photo-induced charge carriers from C_{60} layer would be suppressed by the insulative interfaces [13]. From this point of view, the insertion of BCP layer has been proposed for efficient electron collection [3].

Fig. 5.3(b) shows the *J-V* curves of the evaporation- and the lamination-type devices with the layer structure ITO/ZnPc (30 nm)/C_{60} (40 nm)/BCP (10 nm)/Au (100 nm). In the range of bias between V= 0 and V_{oc}, corresponding to the operating regime of the solar cell, the current density of the lamination-type device was slightly higher than that of the evaporation-type device. In **Table 5.1**, the PV performances of the devices are summarized together with those of the devices without BCP.

It can be seen that the PV performances of the evaporation- and lamination-type devices are effectively improved by insertion of the BCP layer. These results indicate that the BCP layer successfully provided the ETL functions, i.e., transporting electrons to the cathode from the adjoining acceptor layer, while effectively blocking excitons in the lower-energy-gap acceptor layer from recombining at the cathode. Although the FF is inferior to that of the evaporation-type device, the lamination-type device with BCP exhibited the best PV performance with J_{sc} = 4.46 mAcm^{-2} and η_p = 0.467 %. It should be noticed that the BCP layer inserted in the lamination-type device has no defect states originated from the vapor deposition process to form the cathode metal layer. The relatively large J_{sc} and η_P observed with the lamination-type device suggest that the formation of the defect states below the LUMO of BCP postnatally induced by the thermalization of the hot metal atoms [14] would not be necessarily requisite for efficient charge transport across the BCP layer.

Considering the substantial energy gap between the C_{60} and the BCP LUMO levels, it seems inexplicable that the efficient electron transport

predominantly occurs through the LUMO of BCP. However, LUMO levels are apparently variable when interfacial dipoles induced by heterogeneous contacts with different materials. Tanaka *et al.,*[15] investigated the effect of insertion of BCP at Au-ZnPc interface on the energy level alignment of each layer. From the results of UPS, they estimated that the vacuum level shift at the Au/BCP was about -0.4 eV. Sakurai *et al*., also studied the energy band structures at the Au-BCP interfaces by using UPS [16]. They observed a larger shift of the vacuum level, -1.6 eV, that occurs at the interface. Toyoshima *et al.,* formally defined 3.6 eV of pseudo WF of BCP deposited on Au surface [17]. The WF of Au (*ca.* 5.0 eV) is higher than the pseudo WF of BCP. An immediate downward shift in the vacuum level, corresponding to the formation of an interface dipole with its positive pole toward the BCP layer, should be caused by contacting BCP with a higher WF metal.

Conclusion

The interfacial dipoles causing an abrupt shift in energy levels of an organic semiconductor can take place not only at metal-organic interfaces but also at organic-organic interfaces [14,15,18,19]. Recently, Wang *et al.,* [7] reported a dependence of the electronic properties of C_{60}/BCP/Ag heterostructures on the thickness of the BCP layer. They estimated the vacuum level shift of +0.4 eV at the BCP-C_{60} interface from UPS spectra of C_{60} layers deposited on BCP (5nm)/Ag stack layer. The polarities of the vacuum level shifts are considered to reflect the direction of the interfacial dipoles. If vacuum level shifts of +0.4 and -0.4 eV take place at the BCP-C_{60} and Au-BCP interfaces within the multistacking structures of our organic PV cells, as suggested by Wang *et al.,* and Tanaka *et al.,* [7,15] respectively, the height of the energy barrier for electron collection from C_{60} to Au cathode corresponding to the LUMO level of BCP should become as low as 0.6 eV. Alternatively, if the larger vacuum level shifts suggested by *Sakurai et al.,* [16] takes place at the Au-BCP interface, the

interfacial dipole to shift the potential of -1.6 eV reduces the apparent WF of cathode Au. As shown in our previous report [20] the difference between the WFs of cathode and anode is one of the critical elements in determining the performance of an organic PV cell. From this point of view, the vacuum level shift at the Au-BCP interface would be also an important factor to understand the effect of insertion of BCP.

References

1. C. W. Tang, Appl. Phys. Lett. **48**, 183 (1986).
2. G. Yu, J. Gao, J. C. Hummelen, F. Wudl, A. J. Heeger, Science **270**, 1789 (1995).
3. Z. R. Hong, Z. H. Huang, X. T. Zeng, Thin Solid Films **515**, 3019 (2007).
4. P. Peumans, S. R. Forrest, Appl. Phys. Lett. **79**, 126 (2001).
5. T. Oida, K. Harafuji, Jpn. J. Appl. Phys. **51**, 091601 (2012).
6. T. Oida, T. Naito, Y. Miyagawa, M. Sasaki, K. Harafuji, Jpn. J. Appl. Phys. **50**, 081601 (2011).
7. S. Wang, T. Sakurai, R. Kuroda, K. Akimoto, Appl. Phys. Lett. **100**, 243301 (2012).
8. N. Bowden, S. Brittain, A. G. Evans, J. W. Hutchinson, G. M. Whitesides, Nature, **393**, 146 (1998).
9. H. O. Jacobs, G. M. Whitesides, Science. **291**, 1763 (2001).
10. H. Gommans, B. Verreet, B. P. Rand, R. Muller, J. Poortmans, P. Heremans, J. Genoe, Adv. Funct. Mater. **18**, 3686 (2008).
11. M. Vogel, S. Doka, C. Breyer, M. C. Lux-Steiner, K. Fostiropoulos, Appl. Phys. Lett. **89**, 163501 (2006).
12. Z. R. Hong, Z. H. Huang, X. T. Zeng, Chem. Phys. Lett. **425**, 62 (2006).
13. A. J. Maxwell, P. A. Brühwiler, D. Arvanitis, J. Hasselström, M. K.-J. Johansson, N. Mårtensson, Phys. Rev. B **57**, 7312 (1998).
14. G. Parthasarathy, P. E. Burrows, V. Khalfin, V. G. Kozlov, S. R. Forrest, Appl. Phys. Lett. **72**, 2138 (1998).

15. S. Tanaka, Y. Yoshida, M. Nonomura, K. Yoshino, I. Hiromitsu, Thin Solid Films, **516**, 1006 (2008).

16. T. Sakurai, S. Toyoshima, H. Kitazume, S. Masuda, H. Kato, K. Akimoto, J. Appl. Phys. **107**, 043707 (2010).

17. S. Toyoshima, K. Kuwabara, T. Sakurai, T. Taima, K. Saito, H. Kato, K. Akimoto, Jpn. J. Appl. Phys. **46**, 2692 (2007).

18. P. Vivo, J. Jukola, M. Ojala, V. Chukharev, H. Lemmetyinen, Sol. Energy Mater. Sol. Cells, **92**, 1416 (2008).

19. J. Bandara, K. Shankar, C. A. Grimes, M. Thelakkat, Thin Solid Films **520**, 582 (2011).

20. K. Sarangerel, C. Ganzorig, M. Fujihira, M. Sakomura, K. Ueda, Chem. Lett. **37**, 778 (2008).

Figures and tables

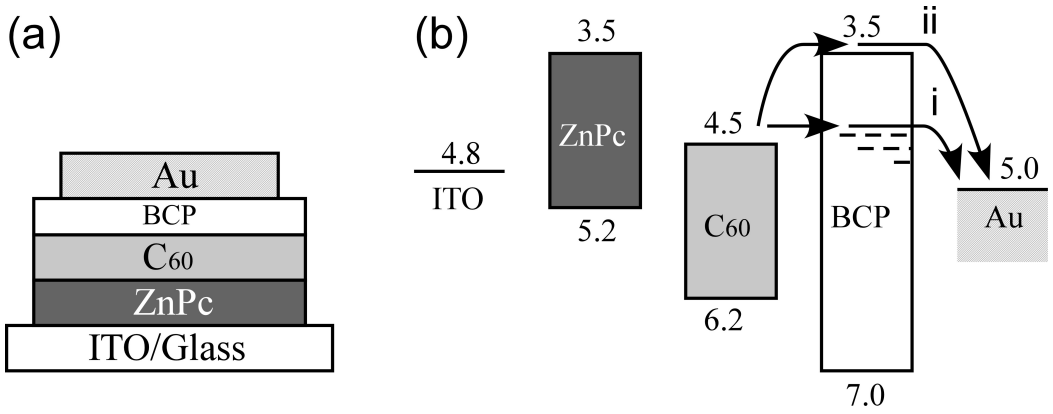

Figure 5.1 Structure of small-molecule organic PV cell with sequentially deposited ZnPc, C_{60}, and BCP layers (a), and the corresponding energy-level diagram showing Fermi levels of electrodes and HOMO and LUMO levels of organic layers (b).

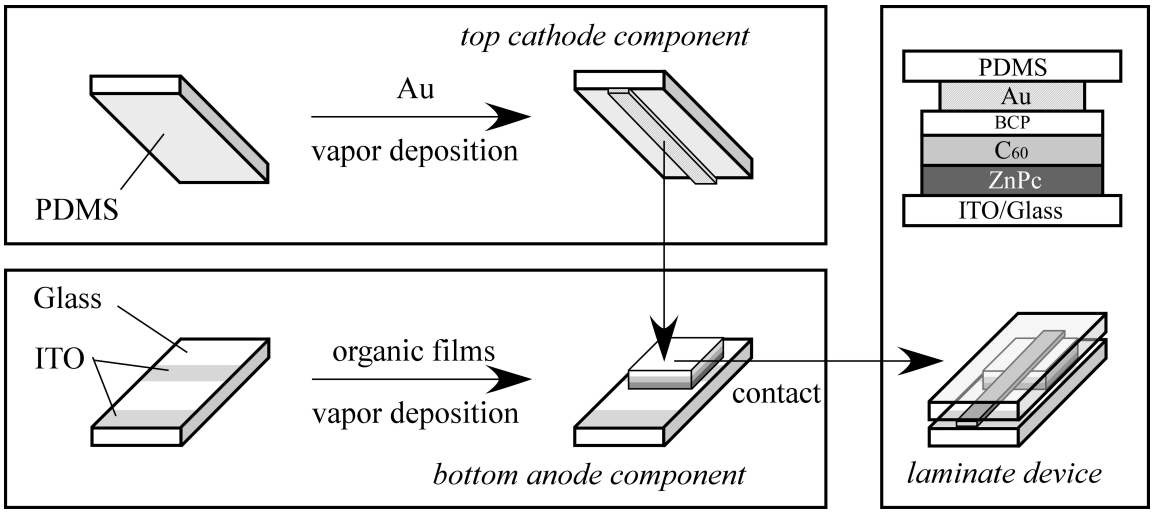

Figure 5.2 Fabrication procedures of laminate organic PV cell.

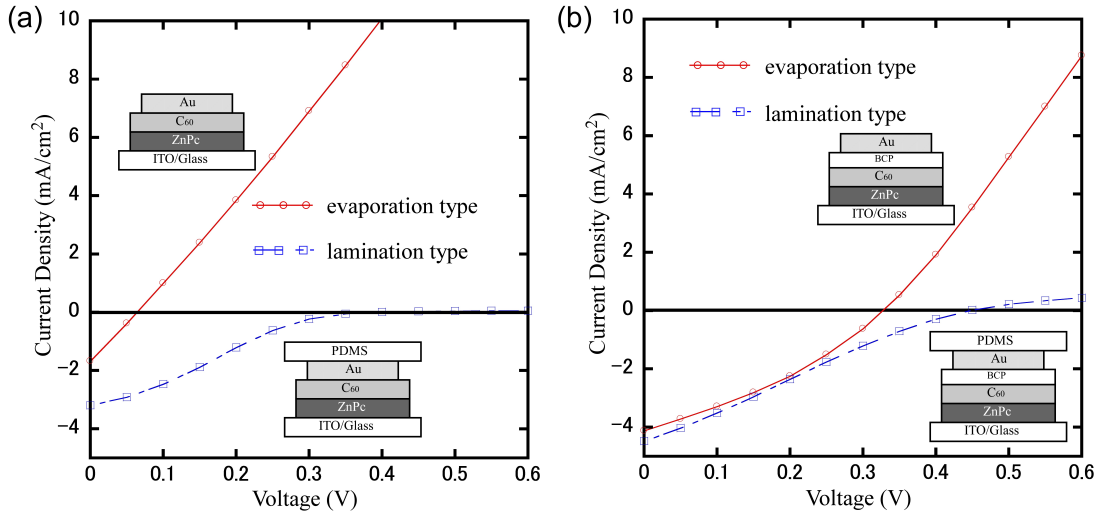

Figure 5.3 *J-V* characteristics for evaporation- and laminationtype organic PV cells without (a) and with (b) BCP buffer layer.

Table 5.1 V_{oc}, J_{sc}, and η_P, as determined from *J-V* characterization in Fig. 5.3

Device	J_{sc} (mAcm^{-2})	V_{oc} (V)	*FF*	η_P (%)
Evaporation without BCP	1.65	0.064	0.255	0.027
Lamination without BCP	3.20	0.374	0.235	0.280
Evaporation with BCP	4.12	0.328	0.333	0.450
Lamination with BCP	4.46	0.451	0.232	0.467

Chapter 6

Summary

Indium-tin-oxide (ITO) is often used as a hole-collecting electrode in organic PV cells. However, the WF of ITO is typically from 4.5 to 4.7 eV, smaller than the highest occupied molecular orbital (HOMO) level of most organic donor materials, which could have a problem for the construction of ohmic contact. In order to realize higher V_{oc}, determined by the energy level offset between the HOMO of the donor and the lower unoccupied molecular orbital (LUMO) of the acceptor, the WF of electrode, and the HOMO of the donor should be matched in the manner of ohmic contact. The ohmic contact also allows the efficient charge collection at the ITO/photoactive layer interfaces and to reduce contact resistance for high J_{SC} and fill factor (FF). In this thesis self-assembly of dipolar molecules onto ITO was examined to achieve the energy level tuning at ITO anode interface. The importance of energy level tuning at the metal cathode interface is essentially the same as that at the ITO anode interface. It has been known that the insertion of a thin organic layer (5-10 nm thickness) of tris(8-hydroxyquinoline)aluminum (Alq_3) or bathocuproine (BCP) as a buffer layer between the metal cathode and organic active layer would induce thae shift of the vacuum level at the cathode interface due to dipole layer formation. The effects of the buffer layers of none doped and doped with Li were also compared. This thesis consists of 6 chapters.

Chapter 1.

General background of the study of organic photovoltaic (PV) cells has been described with in connection with the contents of the thesis.

Chapter 2.

The organic (PV) cells were fabricated with the cell configuration of ITO/zinc phthalocyanine (ZnPc) (40 nm)/fullerene (C_{60}) (40 nm)/ with and without bathocuproine (BCP) (10 nm) between C_{60} and Al by physical vapor deposition. By the use of *para*-substituted benzenesulfonyl chlorides with different terminal groups of H- and Cl-, the energy offset at the ITO/ZnPc interface was fine-tuned widely depending upon the interface dipoles and thus correlation between the change in the ITO work function and the performance of the organic PV cells by chemical modification is examined. The results suggested that the work function of ITO chemically modified with H- and Cl-terminated benzenesulfonyl chlorides were shifted down to the HOMO level of ZnPc resulting in formation of ohmic contact at the ITO/ZnPc interface.

Chapter 3.

The effect of chemical modification of ITOs with CH_3O-, H-, Cl-, CF_3-, and NO_2-terminated *p*-benzenesulfonyl chlorides on the PV characteristics of bulk-heterojunction BHJ solar cells based on poly(3-hexylthiophene) and [6,6]-phenyl-C_{61}-butyric acid methyl ester (P3HT:$PC_{61}BM$) composite structure were examined. The ITO electrode surfaces were easily treated through the chemical modification of the reactive –SO_2Cl binding group, and the WF of the modified ITO were effectively changed depending on the permanent dipole moments introduced in the *para*-position of benzenesulfonyl chloride. We examined the correlation between the ITO WFs corrected by the change in the contact potential difference and the calculated dipole moments of the SAM models. Moreover, we examined the PV characteristics of the P3HT:$PC_{61}BM$ based BHJ organic PV cells using the SAMs or poly(3,4-ethylenedioxythiophene):poly(styrene sulfonate) (PEDOT:PSS)-treated ITOs with different WFs lying within ±0.2 eV from the HOMO level of P3HT. We found that the enhancement effect of the SAMs on the h_P reached a maximum with Cl (h_P = 3.72 %), and became larger

than that of PEDOT:PSS (h_P = 3.62 %). Two distinct J_{sc} dependencies, increasing and decreasing with the increasing WF of the anode ITO, were observed at higher and lower WFs than the HOMO level of the donor, respectively. Almost constant V_{oc} values (around 0.6 V) were observed with different SAM-modified ITOs, which suggested that Fermi level pinning was achieved by aligning the anode Fermi level and positive polaronic level of the donor polymer.

Chapter 4.

The effects of insertion of dipolar SAMs and buffer layers of BCP and Alq_3 at the interfaces of ITO anode and Al cathode electrodes, respectively, on the PV performances of rubrene/C_{60}/ based organic PV cells were examined. Moreover, the effects of Li doped buffer layers were also examined. In order to enhance built-in potential (V_{bi}), which is generally related to the V_{oc} should be increased and WF of Al should be decreased. The correlation between the change in WFs of electrodes and performance the organic PV cells before and after surface modifications was examined in detail.

Chapter 5.

BCP has been known as one of the most effective electron-transport layer material, however, the mechanism of the electron transport is not clear yet. In order to clarify this, we examined the organic PV cells of ITO/ZnPc/C_{60}/BCP/Au formed with a laminated top electrode to suppress cathode-induced defect states in the BCP layer. The results indicated that the formation of the cathode-induced defect states below the LUMO of BCP would be not be necessarily requisite for efficient charge transport across the BCP layer. In conclusion, the efficient electron transport should be via LUMO energy level of BCP. The vacuum level shifts at the Au-BCP and BCP-C_{60} interfaces were considered to be important factors to understand the effective electron transport via the LUMO of BCP layer.

Chapter 6.

All the results of the research work were summarized in this chapter.

List of Publications

1. Delgertsetseg Byambasuren, Sarangerel Khayankhyarvaa, Javkhlantugs Namsrai, Sakomura Masaru, Ueda Kazuyoshi, Ganzorig Chimed, Improved performances of organic solar cells with ITO electrodes treated by molecular self-assembly", Rev. Téc. Ing. Univ. Zulia. **37**, 35 (2014). (Chapter 2)
2. Byambasuren Delgertsetseg, Namsrai Javkhlantugs, Erdenebileg Enkhtur, Yuya Yokokura, Takayuki Ooba, Kazuyoshi Ueda, Chimed Ganzorig, Masaru Sakomura, "Detailed investigation of dependencies of photovoltaic performances of P3HT:PC61BM based solar cells on anodic work function modified by surface treatment of indium-tin-oxide electrode with benzenesulfonyl chloride derivatives, Organic Electronics, **23** 164 (2015). (Chapter 3)
3. Khayankhyarvaa Sarangerel, Byambasuren Delgertsetseg, Namsrai Javkhlantugs, Masaru Sakomura, and Chimed Ganzorig, "Improvement of Open-Circuit Voltage in Organic Photovoltaic Cells with Chemically Modified Indium-Tin Oxide", World Journal of Nano Science and Engineering. **3**, 113 (2013), (Chapter 4)
4. Masaru Sakomura, Minoru Matsushiro, Masaya Sawayama, Shima Miura, Byambasuren Delgertsetseg, Chimed Ganzorig, and Kazuyoshi Ueda, "Effect of Bathocuproine Electron-Transport Layer in Small Molecule Solar Cells with Laminated Top Electrode", Chemistry Letters. **42**, 1179 (2013), (Chapter 5)

Acknowledgements

All staffs whose assistance and contribution were invaluable for the Japan Society for Promotion of Science (JSPS) RONPAKU (Dissertation PhD) Program (2010-2015).

The author is indebted to Professor Masaru Sakomura for his invaluable comments, fruitful discussions, his constant encouragement, assistance, and patience throughout this study. The author would like to thank Professors Chimed Ganzorig and Kazuyoshi Ueda for their kind advice, suggestions and assistance in the production of this research work in a field of Organic Photovoltaic Materials and Cells.

The author also would like to appreciate Doctors Namsrai Javkhlantugs and Khishigjargal Tegshjargal, and Yuya Yokokura for their fruitful advice and experimental assistance.

The author also would like to thank all the members of the Ueda-Sakomura laboratory for their experimental, technical and theoretical suggestions, their profitable discussions and for their kind cooperation.